[AMERICAN JOURNAL OF SCIENCE, VOL. 300, DECEMBER, 2000, P. 723–767]

American Journal of Science

DECEMBER 2000

TERTIARY SEAWATER CHEMISTRY – IMPLICATIONS FROM PRIMARY FLUID INCLUSIONS IN MARINE HALITE

HEIDE ZIMMERMANN

Department of Earth and Planetary Sciences, Harvard University, 20 Oxford Street, Cambridge, Massachusetts 02138

ABSTRACT. Most reconstructions of the chemistry of seawater during the Phanerozoic are based on the mineralogy of marine evaporites or on the composition of fluid inclusions in such evaporites. This paper reviews the data for the composition of primary fluid inclusions in halite from Tertiary marine evaporites in an effort to define the composition of seawater during the past 40 Ma. Four sets of primary fluid inclusion data from 130 sedimentary halite samples are currently available from the Eocene (37 Ma) Navarra Basin in Spain, the Oligocene (35 Ma) Mulhouse Basin in France, the Lower to Middle Miocene (14 Ma) evaporite deposits of the Carpathian region in Eastern Europe, and the Upper Miocene evaporites (5 Ma, Messinian) of the Mediterranean and the Red Sea.

The composition of the primary inclusion fluids in these evaporites cannot be explained in terms of the simple evaporation of modern seawater. Many inclusion brines are the result of potash mineral precipitation or recycling of evaporites. About half the fluid inclusions analyzed can be interpreted as evaporated seawater depleted in $MgSO_4$. Eocene and Oligocene inclusion fluids indicate Mg-depletions of 32 and 36 percent compared to modern seawater, which agrees well with the mineralogy of the potash zones (sylvite, carnallite) in these evaporites. The Badenian inclusion fluids show a Mg-depletion of 20 percent and the Messinian inclusion brines a Mg-depletion of 12 percent, which is consistent with the composition of the potash zones (kainite) in these evaporites.

The $MgSO_4$-depletion of these inclusion fluids is either due to the dolomitization of limestone during the evaporative concentration of modern seawater, to changes in the composition of seawater during the Tertiary, or due to a combination of these effects. Analyses of fluid inclusions containing unevaporated seawater are needed to determine the cause of the observed $MgSO_4$-depletion. Fluid inclusions in early marine calcite cements may help to resolve the issue.

INTRODUCTION

Although many efforts have been made to constrain the composition of seawater during the Phanerozoic, it is not yet well defined. Most reconstructions of the chemistry of seawater during the Phanerozoic are based on the mineralogy of marine evaporites or on the composition of fluid inclusions in such evaporites. As long as no complete chemical analyses of unevaporated seawater are available (Johnson and Goldstein, 1993), we are limited to analytical data of fluid inclusions such as in halite from marine evaporative settings to constrain the composition of seawater during the Phanerozoic.

Primary fluid inclusions along growth bands in chevron and cumulate crystals in sedimentary halite are most suitable for the reconstruction of the composition of Phanerozoic seawater, because they contain brines from the initial sedimentary basin. These primary fluid inclusions can be identified based on petrogaphic and sedimentological criteria (Goldstein and Reynolds, 1994; Benison and Goldstein, 1999). How-

ever, the brine preserved from the initial evaporite basin is not necessarily simply evaporated seawater prior to potash facies, which is needed to constrain the chemistry of contemporaneous unevaporated seawater. In certain evaporite basins the input of non-marine waters can be considerable. Brine mixing and recycling of halite may occur. The absence of potash salts in the record of a marine halite sequence does not necessarily mean that potassic minerals were not precipitated in the sedimentary basin. They may have been precipitated and later redissolved due to the inflow of less concentrated brines.

Petrographic studies of the sedimentary fabric and of the spatial distribution of fluid inclusions are not sufficient to identify among the primary fluid inclusions the ones that contain moderately evaporated seawater (that is, prior to potash facies). Additional geochemical screening is necessary to select this type of primary fluid inclusions and to check them against the proposed models of Phanerozoic seawater composition. Strategies for the geochemical screening are described more in detail by Zimmermann (2000a). This paper reviews the data for the compositions of primary fluid inclusions in chevron and cumulate halite from Tertiary marine evaporites in an effort to define the evolution of the chemistry of seawater during the past 40 Ma.

METHOD

The Jänecke diagram of the NaCl-KCl-$MgCl_2$-Na_2SO_4-H_2O system at 25 °C

The validity of some of the proposed changes in seawater composition during the Phanerozoic can be tested with the help of the Jänecke-plot of the NaCl-KCl-$MgCl_2$-Na_2SO_4-H_2O or NaCl-KCl-$MgCl_2$-$CaCl_2$-H_2O-system. Though originally established to quantify the precipitation and reaction of potash minerals in NaCl-saturated systems (calcium carbonate and calcium sulfate are already removed; see Althammer, 1924; D'Ans, 1933; Braitsch, 1962; Peters, 1988, Usdowski and Dietzel, 1998), the Jänecke units Mg, 2K, SO_4 or Ca, m(H_2O), and 2NaCl also give important information for brines that are less evaporated (Zimmermann, 2000a).

The NaCl-KCl-$MgCl_2$-Na_2SO_4-H_2O system can be considered as three substituting salt pairs, each of which forms a subsystem that can be described in terms of a square (fig. 1, step 1):

$$2NaCl + MgSO_4 = Na_2SO_4 + MgCl_2$$

$$MgCl_2 + K_2SO_4 = MgSO_4 + 2KCl$$

$$2KCl + Na_2SO_4 = K_2SO_4 + 2NaCl$$

Because all these squares share one side each, they can be set up as a prism with the chlorides at the bottom and the sulfates on top (fig. 1, step 2). Assuming saturation of the brines with NaCl, the Na_2Cl_2 component can be projected from the prism corner along the adjunct sides of the squares Na_2Cl_2-$MgCl_2$-Na_2SO_4-$MgSO_4$ and Na_2Cl_2-K_2Cl_2-Na_2SO_4-K_2SO_4 and of the bottom triangle Na_2Cl_2-K_2Cl_2-$MgCl_2$ (fig. 1, step 3). These projections define the three sides Mg- SO_4, SO_4-2K, and 2K-Mg of a triangle (fig. 1, step 4) which is called the Jänecke diagram.

If for an example one assumes a brine composition of 14.2 mole $MgCl_2$/1000 mole H_2O, 19.1 mole $MgSO_4$/1000 mole H_2O, and 11.6 mole K_2Cl_2/1000 mole H_2O, this gives 33.3 mole Mg/1000 mole H_2O, 19.1 mole SO_4/1000 mole H_2O, and 11.6 mole 2K/1000 mole H_2O. Transformed into mole percent this results in the Jänecke units of 52 mole percent Mg, 30 mole percent SO_4, and 18 mole percent 2K. m(H_2O) is defined as mole water per 100 mole Σ (Mg + SO_4 + 2K). In this case m(H_2O)=

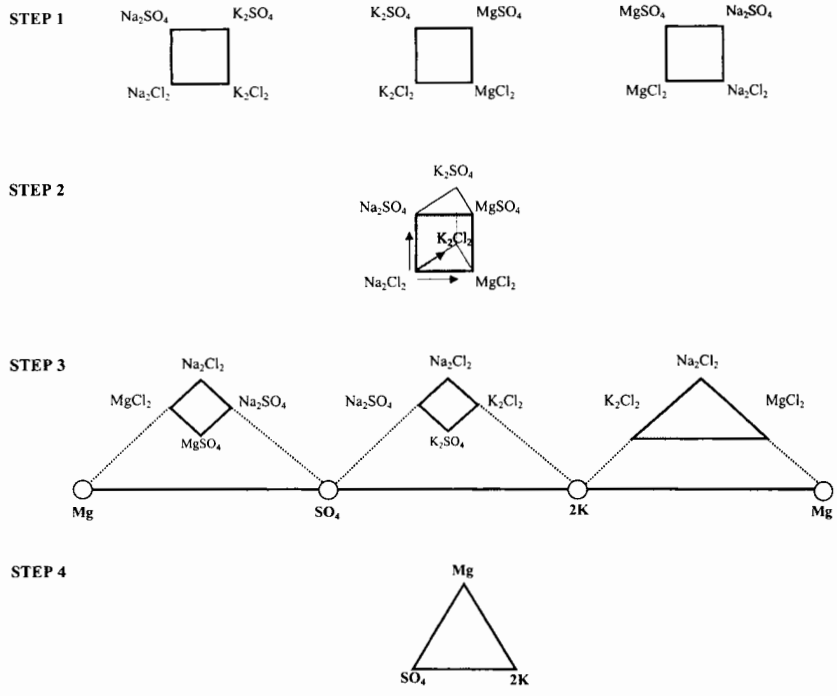

Fig. 1. The Jänecke projection of the NaCl-KCl-$MgCl_2$-Na_2SO_4-H_2O system. For details see for example, Althammer, 1924; Usdowski and Dietzel, 1998.

1000*100/64.0, which is 1563. Similar to $m(H_2O)$ the 2NaCl-value refers to mole 2NaCl per 100 mole Σ (Mg + SO_4 + 2K).

Models of Phanerozoic seawater in the Jänecke diagram of the NaCl-KCl-$MgCl_2$-Na_2SO_4-H_2O system at 25 °C

Unevaporated *seawater of modern composition* in the Jänecke-diagram at 25°C projects in the stability field of bloedite (mSW, fig. 2), though its water value of $m(H_2O)=70700$ is well above the saturation surface at $m(H_2O)=1260$. Prior to potash mineral precipitation the relative ratio of Mg, 2K, and SO_4 of evaporated seawater (Mg=69.0, 2K=6.5, SO_4=24.5 mole percent) remains constant. Therefore all points representing the composition of evaporated seawater prior to potash mineral precipitation fall on the projection point of modern seawater (mSW, fig. 2). The $m(H_2O)$ values of halite saturated seawater at 10 times and 60 times the concentration of modern seawater (=prior to potash facies) are 7070 and 1260, the 2NaCl values 305 and 22 respectively (Zimmermann, 2000a). This would also apply to inclusions of simply evaporated seawater in ancient marine halite if seawater composition had not changed during the Phanerozoic. Higher $m(H_2O)$- and 2NaCl values usually indicate brine mixing and recycling of halite.

Holland (personal communication) has suggested that the *molar Mg/Ca-ratio in global seawater* during parts of the Paleozoic might have been *twice the present value* of 5. If the sum of the concentration of calcium and magnesium was the same as today, seawater with a molar Mg/Ca-ratio of 10 would plot on the unfilled square in the Jänecke-diagram ($SW_{Mg/Ca}=10$, fig. 2). Assuming a variation in molar Mg/Ca-ratios of initial seawater between 5 and 10, primary fluid inclusions of simply evaporated

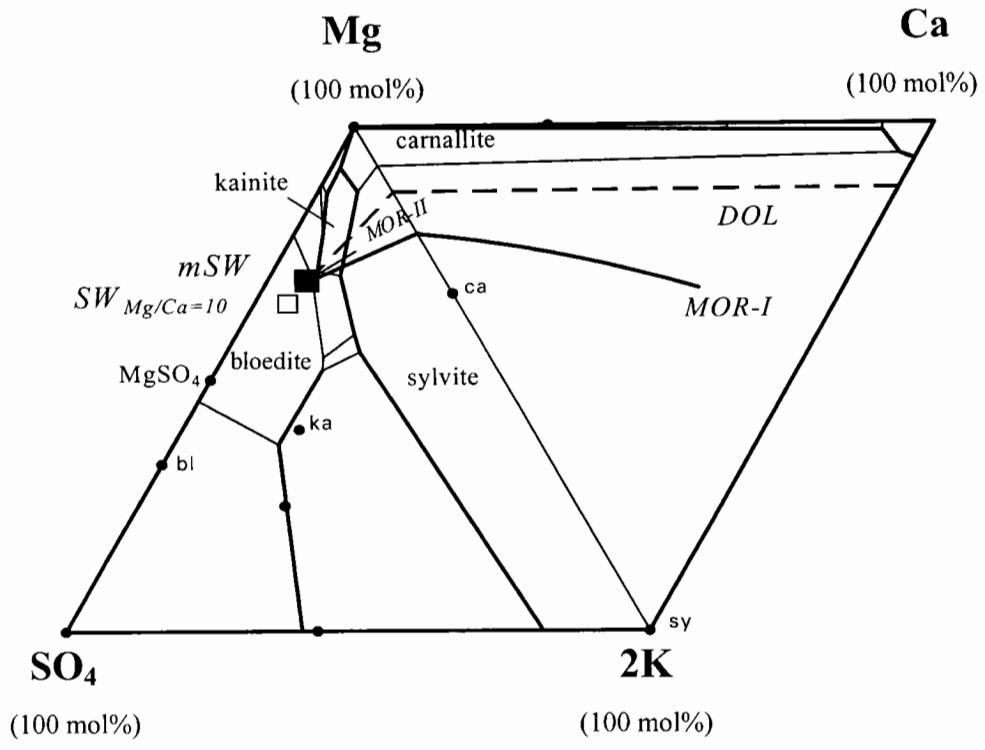

Fig. 2. Models of Phanerozoic seawater chemistry plotted in the Jänecke diagram of the NaCl-KCl-$MgCl_2$-Na_2SO_4-H_2O/NaCl-KCl-$MgCl_2$-$CaCl_2$-H_2O system at 25 °C. Black filled circles mark plotting points of solid phases: bl=bloedite, ca=carnallite, ka=kainite, sy=sylvite. Stability fields of solid phases are labeled by the names of their mineral.

mSW = plotting point of modern seawater, black filled square; $SW_{Mg/Ca=10}$ = plotting point of seawater with an initial Mg/Ca-ratio of 10; *MOR-I* = predicted seawater chemistry for variations in sea floor spreading rates according to Hardie (1996 and personal communication); *MOR-II* = predicted seawater chemistry, if affected by variations in sea floor spreading rates, according to Holland, Horita, and Seyfried (1996); *DOL* = predicted chemistry of seawater affected by the dolomitization of limestones during evaporative concentration.

seawater should plot on a straight line that connects the unfilled square of seawater with a Mg/Ca-ratio of 10 to the plotting point of modern seawater (fig. 2).

If the composition of *seawater* had *changed due to variations in seafloor spreading rates at mid-ocean ridges* as predicted by Hardie (1996 and personal communication), primary fluid inclusions of evaporated seawater in ancient halite (prior to potash mineral precipitation) should plot on the black line MOR-I in figure 2. Holland, Horita, and Seyfried (1996) recalculated the effect of variations in spreading rates on global seawater composition resulting in a far more modest change in global seawater composition (MOR-II, fig. 2). Verifying their estimates turns out to be more difficult, because the calculated trend is to some extent similar to the effects on seawater composition caused by the dolomitization of limestones (see below). However, both suggested models might be of minor importance for the evolution of the chemistry of the oceans during the Tertiary, because the rate of seafloor spreading did not change significantly during the past 40 Ma (fig. 3; Lithgow-Bertelloni and others, 1993; Heller, Anderson, and Angevine, 1996).

It was also pointed out that the composition of *seawater in evaporative settings* can be seriously *affected by the dolomitization of limestone* during evaporative concentration

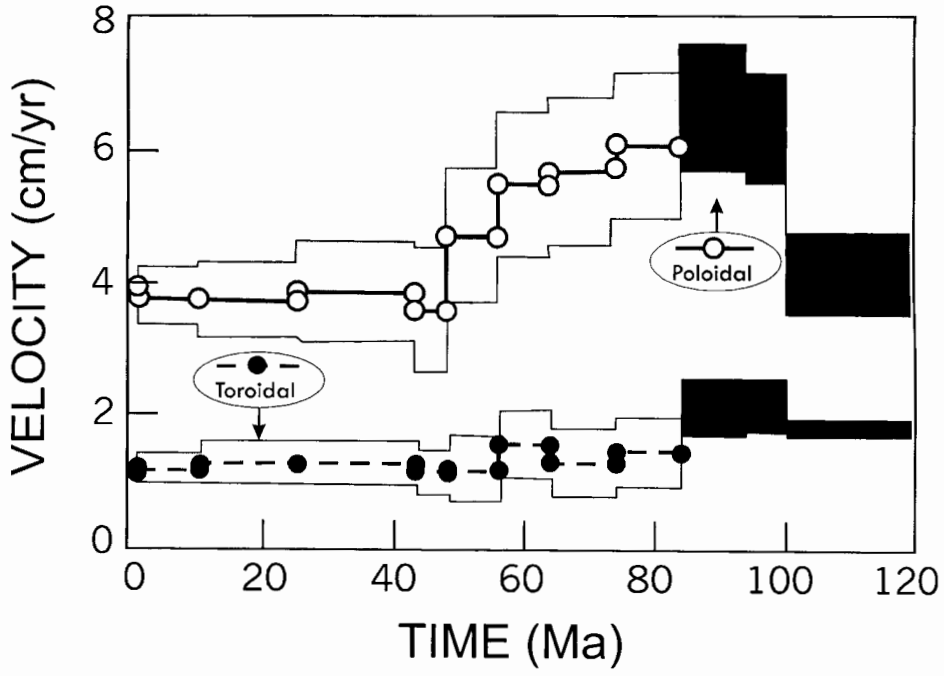

Fig. 3. Toroidal and poloidal rates of seafloor spreading during the past 120 Ma (Lithgow-Bertelloni, and others, 1993).

without the need for major changes in global seawater composition (Braitsch, 1962; Das, Horita, and Holland, 1990; Williams-Stroud, 1994; Holland, Horita, and Seyfried, 1996; Holland and Zimmermann, 1998). Assuming that the initial seawater composition was similar to the modern one, dolomitization of limestones would affect seawater chemistry in the following way: While magnesium is removed from modern seawater to form dolomite, an equal amount of calcium is released from the reacting limestone. The excess calcium combines with dissolved seawater sulfate to form gypsum, the net balance of the whole process being an equimolar removal of magnesium and sulfate. The composition of seawater, modified due to this process (*DOL*, fig. 2), plots along a line toward the 2K-Mg side of the Jänecke diagram, moving directly away from the projection point of $MgSO_4$. If magnesium is depleted by more than 35 percent of that in modern seawater, there is not enough seawater sulfate to precipitate all the released calcium, and $CaCl_2$ will build up in the evaporated brine. The modified seawater compositions then plot along a line toward the 2K-Ca side of the Jänecke diagram (*DOL*, fig. 2). Seawater with higher initial Mg/Ca-ratios and seawater modified due to changes in spreading rates according to Holland, Horita, and Seyfried (1996), which is affected by dolomitization, would also lead to seawater compositions along the dashed line (*DOL*) in figure 2. The depletion in magnesium relative to modern seawater due to the dolomitization of limestones can be estimated on the basis of Mg and K concentrations in fluid inclusions or based on the mineralogy of primary potash beds (for details see Zimmermann, 2000a).

Screening of primary inclusion fluids for evaporated seawater prior to potash facies based on $DE_{ELEMENT}$ *patterns*

The evaporation path for modern seawater is well known from numerous field studies (Herrmann and others, 1973; Busson and others, 1982; Brantley and others,

1984; McCaffrey, Lazar, and Holland, 1987; Isele, 1998). It also can be predicted on the basis of the Harvie-Møller-Weare-model (1984) and the solid-solution-equilibria of the NaCl-KCl-$MgCl_2$-Na_2SO_4-H_2O/NaCl-KCl-$MgCl_2$-$CaCl_2$-H_2O system (Usdowski and Dietzel, 1998). This also allows the simulation of the evaporation path of seawater, which is affected by the dolomitization of limestones (depleted in $MgSO_4$ and/or enriched in $CaCl_2$). $DE_{ELEMENT}$ patterns (degree of evaporation for a specific element based on modern seawater composition) of evaporated seawater along this path are calculated. Then $DE_{ELEMENT}$ patterns of primary fluid inclusions in halite are compared to the specific patterns predicted for this kind of evaporated seawater. The degrees of evaporation of seawater for various elements (K, Mg, Br, B, Li, Rb) are calculated using the following equation:

$$DE_{MG} = (\text{mmole Mg/kg } H_2O)_{BRINE}/(\text{mmole Mg/kg } H_2O)_{MODERN\ SEAWATER} \quad (1)$$

Simply evaporated modern seawater, which is trapped in fluid inclusions of marine halite prior to the potash facies, has 10 to 60 times the concentration of the initial seawater (von Borstel, Zimmermann, and Ruppert, 2000; Zimmermann, 2000a). Because no significant amounts of K, Mg, and Br are removed during the precipitation of halite prior to the potash facies, evaporated modern seawater shows the following $DE_{ELEMENT}$ pattern:

$$DE = DE_{BR} = DE_K = DE_{MG}$$

with

$$10 \leq DE \leq 60$$

and

$$DE_{MG}/DE_K = 1$$

The assumption that the concentration of Br in seawater did not change significantly during the past 40 Ma seems justified because of its residence time in the oceans of $\sim 10^8$ a (Holland, 1978). This assumption implies that simply evaporated seawater during the Tertiary prior to potash facies would also have a DE_{BR} between 10 and 60. If the concentration of major species in seawater has changed during the Tertiary and if seawater were depleted in $MgSO_4$, evaporated seawater can reach the saturation with potash minerals at DE's slightly above 60. By choosing a threshold of DE=60 for screening, we risk to accidentally abandon a few primary fluid inclusions, which may contain seawater not yet saturated with potassic salts. However, this is not critical to our purposes, because by this choice we are sure to eliminate all inclusion fluids that are already saturated with potash salts from our selection .

If the composition of Phanerozoic seawater had been modified solely by variations in the degree of dolomitization during the evaporative concentration of seawater, the K content in seawater would not be affected, whereas the concentration of Mg would be less than in modern seawater. Therefore, prior to potash facies this type of evaporated seawater is characterized by:

$$DE = DE_{BR} = DE_K \neq DE_{MG}$$

with

$$10 \leq DE \leq 60$$

and

$$DE_{MG}/DE_K < 1$$

Both evaporated seawater of modern composition and evaporated seawater affected by the dolomitization of limestones typically have a DE_{BR} and DE_{MG} clearly above 60 and a $DE_{MG}/DE_K \gg 1$ when saturated with potash minerals (Zimmermann, 2000a). If the dissolution of potash minerals and brine mixing are involved, fluids may have DE_{BR}, DE_{MG}, and DE_K below 60 and could be mistaken for simply evaporated seawater prior to potash facies. However, they typically show a $DE_{MG}/DE_K \gg 1$ and therefore can be clearly distinguished from simply evaporated seawater (for details, see Zimmermann, 2000a).

Procedure for evaluating compositions of inclusion fluids in halite

The following procedure is applied in this review to evaluate and screen the compositions of inclusion fluids in marine halite:

—The marine origin of the evaporites selected for fluid inclusion studies is evaluated in order to make sure that the evaporated seawater in the basin was not contaminated by potential input from continental waters into the sedimentary basin.

—The occurrence and mineralogy of potash zones within these evaporites and the stratigraphic position of the halite samples within the sequence are studied carefully.

—On the basis of petrographic and sedimentological criteria primary fluid inclusions from growth bands in cumulate and chevron crystals of marine halite are selected.

—Prior to further geochemical screening, Jänecke units are calculated for all the selected primary fluid inclusions. They are plotted in the Jänecke diagram of the NaCl-KCl-$MgCl_2$-Na_2SO_4-H_2O/ NaCl-KCl-$MgCl_2$-$CaCl_2$-H_2O system at 25 °C in order to check whether they fit one of the predicted trends for Phanerozoic seawater composition. (With the analyses of many primary inclusions it is very likely that at least a few among them represent evaporated seawater prior to potash facies.)

—Among these primary inclusions, fluid compositions are selected that fit the $DE_{ELEMENT}$ patterns for evaporated seawater of modern or in magnesium depleted composition prior to potash facies. Analyses of primary fluid inclusions in chevron and cumulate halite are screened for inclusions with DE_K (or better DE_{BR} if Br data are available) between 10 and 60 and $DE_{MG}/DE_K \leq 1$.

—The fluid compositions, which are selected on the basis of these geochemical criteria, are marked in the Jänecke diagram at 25 °C. It is checked, whether these inclusions of moderately evaporated seawater fit the composition of Phanerozoic seawater (*DOL*), whose chemistry is solely affected by variations in the extent of dolomitization of limestones during evaporative concentration (this screening is independent of the calculation of Jänecke units and compositions of fluid inclusions selected on the basis of their $DE_{ELEMENT}$ pattern do not necessarily plot along *DOL*.)

—Based on the knowledge of the evaporation path of seawater prior to potash precipitation (Harvie-Møller-Weare-model; Solid-Solution-Equilibria of the NaCl-KCl-$MgCl_2$-Na_2SO_4-H_2O/NaCl-KCl-$MgCl_2$-$CaCl_2$-H_2O system), some characteristics of the composition of ambient unevaporated seawater are deduced from the chemistry of the fluid inclusions selected.

DATA SETS

Four sets of fluid inclusion data from about 130 individual Tertiary marine halite samples (3-10 inclusions were analyzed per sample) are currently available for the Eocene, the Oligocene, and the Miocene (fig. 4). Only primary fluid inclusions in

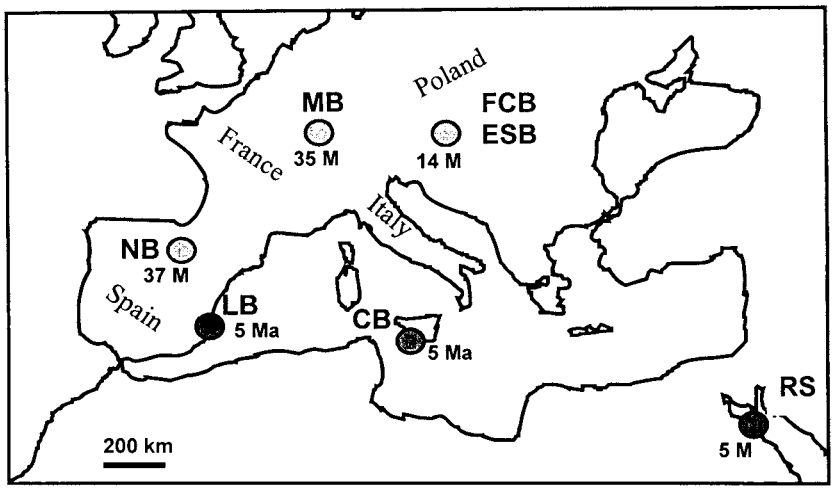

Fig. 4. Map with locations of the Tertiary evaporite basins included in the compilation of fluid inclusion analyses in marine halites. NB=Navarra Basin (Eocene); MB=Mulhouse Basin (Oligocene); FCB=Forecarpathian Basin, ESB=East Slovakian Basin (Badenian); CB=Cattolica Basin, LB=Lorca Basin, RS=Red Sea (Messinian).

sedimentary halite are considered in this review for the reconstruction of the chemistry of seawater.

Primary fluid inclusions in 20 halite samples from the Upper Eocene (~ 37 Ma) of the Navarra Basin in Northern Spain (Ayora, Garçia-Veigas, and Pueyo, 1994a; fig. 4) were analyzed by cryo-EDS-SEM. This technique allows the analysis of Na, K, Mg, Ca, S, and Cl in fluid inclusions >100 μm in size with a precision of 10 to 20 percent (Ayora and Fontarnau, 1990). It does not permit the determination of the concentration of trace elements. Since no analyses of bromine or other trace elements were obtained, the use of $DE_{ELEMENT}$ patterns (only DE_{Mg} and DE_K) is somewhat limited. The second data set is from the Lower Oligocene (~35 Ma) evaporites of the Mulhouse Basin in France (fig. 4). Na, K, Mg, Ca, S, and Cl in primary fluid inclusions of 8 halite samples from the upper part of Salt IV were determined by EDS-SEM and laser ablation ICP-AES (Canals and others, 1993).

The third data set derives from the Badenian (~ 14 Ma, Lower to Middle Miocene) evaporites from Eastern Europe (fig. 4). Cryo-EDS-SEM data of fluid inclusions in 6 halite samples from the Carpathian Foredeep in Poland were analyzed by Garçia Veigas, Rossel, and Garlicki (1997) using the same technique as Ayora, Garçia-Veigas, and Pueyo (1994a). Galamay and Karoli (1997), Galamay, Bukowski, and Przybylo (1997), and Kovalevich and Petrichenko (1997) extracted primary fluid inclusions in 28 samples from the Carpathian Foredeep, in 18 samples from the East Slovakian Basin, in 4 samples from the Transylvanian Basin, and in 2 samples from the Transcarpathian Basin. They used the Petrichenko method (Petrichenko, 1973; Petrychenko, Peryt, and Roulston, 2000) and determined K, Mg, and SO_4 after adding precipitants with a precision of about 20 percent. Unfortunately, this method does not allow the determination of all the main components. The quality of their data cannot be checked by calculating charge balances or by the determination of the degree of saturation with respect to halite. The fluid inclusion analyses of 21 Badenian evaporites from the Transcarpathian Basin by Shaidetska (1997) are not included in this review, because they were extracted from partly recrystallized halite; fluid inclusions in relics of chevrons also seemed to have been affected by recrystallization.

The final data set derives from Messinian (~5 Ma, Upper Miocene) marine halites in the Red Sea and the Mediterranean Sea (Garçia-Veigas and others, 1995; Kovalevich and others; 1997, Shepherd and others, 1998; Lazar and Holland, 1999; Zimmermann, 2000b; see fig. 4). Kovalevich and others (1997) studied the composition of primary fluid inclusions in 8 halite samples from DSDP sites 225 and 227 in the Red Sea using the Petrichenko method. Lazar and Holland (1999) also analyzed fluid inclusions in 11 samples of halite from DSDP 227. They opened fluid inclusions >300 μm in size mechanically with a microdrill, extracted the fluid with a microsyringe, and analyzed Na, K, Mg, Ca, Cl, SO_4, Li, and Br by ion chromatography with an uncertainty of about 2 to 5 percent (Lazar and Holland, 1988). These large inclusions were located next to growth bands with dozens of small inclusions, which range from 1 to 30 μm in length. According to analytical results by T. K. Lowenstein and J. Horita (personal communication) many of these large inclusions next to growth bands have the same fluid composition as the smaller inclusions within the growth bands.

Garçia-Veigas and others (1995) analyzed primary fluid inclusions in 11 halite samples from the Cattolica Basin in Sicily and in 14 samples from the Lorca Basin in Southern Spain. Two of the latter were additionally analyzed by laser ablation ICP-MS (Shepherd and others, 1998). The use of laser ablation ICP-MS for fluid inclusions > 20 μm in length yields elemental ratios for some of the major ions and for Br, B, Sr, Li, and Rb, elements that serve as important geochemical tracers (Shepherd and Chenery, 1995). The analytical error varies between 10 and 30 percent. The application of the Jänecke diagram and of $DE_{ELEMENT}$ patterns requires the determination of element concentrations of inclusion fluids. Therefore laser ablation ICP-MS measurements need to be externally calibrated, for example by cryo-EDS-SEM. Laser ablation ICP-MS and cryo-EDS-SEM data for primary fluid inclusions in 4 additional samples from the Realmonte mine in Sicily are reported in Zimmermann (2000b).

RESULTS

Figure 5 presents the compositions of all primary fluid inclusions (selected on the basis of petrographic criteria) in Tertiary marine halite in a Jänecke diagram at 25 °C prior to further geochemical screening. There is a considerable range in the compositions of these primary fluid inclusions. As mentioned above, it is very likely that at least a few among the many individual primary fluid inclusions in Tertiary marine halite, which were analyzed, contain evaporated seawater prior to potash facies and possibly follow one of the predicted trends for Phanerozoic seawater. The compositions of the analyzed primary fluid inclusions do not simply scatter around the black square representing modern seawater (*mSW*, fig. 5) or plot next to the composition of seawater with a higher Mg/Ca-ratio ($SW_{Mg/Ca}=10$, fig. 5). Neither do they follow the well-understood pathway for strongly evaporated modern seawater. The compositions of only very few fluid inclusions fit the *MOR-I* trend (fig. 5). Among the predicted models for Phanerozoic seawater the dolomitization model (*DOL*, fig. 5) seems the most compelling, and quite a few compositions of fluid inclusions plot along the dolomitization path in the Mg-2K-SO_4 part of the Jänecke-diagram. However, there are also many compositions of primary fluid inclusions, that plot in the upper part of the Jänecke diagram at some distance from the path of seawater affected by dolomitization. To check the dolomitization model for Phanerozoic seawater (*DOL*) time-resolved geochemical screening by $DE_{ELEMENT}$ patterns is required, to select from the primary fluid inclusions the ones that contain simply evaporated and Mg-depleted seawater prior to potash facies. In the following sections, compositions of inclusion fluids in halites from Eocene, Oligocene, Badenian, and Messinian evaporite basins are separately evaluated according to the procedure described above.

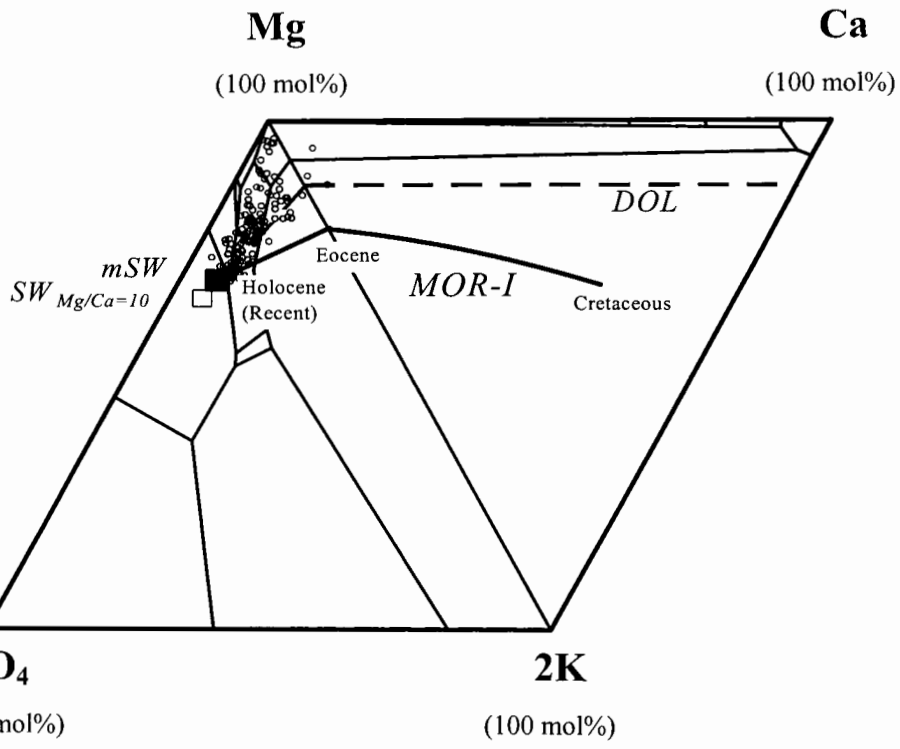

Fig. 5. Compositions of all primary fluid inclusions (unfilled circles) in Tertiary marine halites plotted in the Jänecke diagram of the NaCl-KCl-$MgCl_2$-Na_2SO_4-H_2O/NaCl-KCl-$MgCl_2$-$CaCl_2$-H_2O system at 25 °C.
mSW = plotting point of modern seawater, black filled square; $SW_{Mg/Ca=10}$ = plotting point of seawater with an initial Mg/Ca-ratio of 10; *MOR-I* = predicted seawater chemistry for variations in sea floor spreading rates according to Hardie (1996 and personal communication); *DOL* = predicted chemistry of seawater affected by the dolomitization of limestones during evaporative concentration.

Eocene

The evolution of the Upper Eocene Navarra evaporite basin in Northern Spain (fig. 4) is related to the uplift of the Pyreneen chain. Two evaporitic episodes fed by marine sources developed during the Eocene in the south Pyrenean foredeep basin (Ortí, 1997; Rosell and Pueyo, 1997). Both phases display many characteristics of deep basinal evaporites and developed at the end of well-defined marine sedimentary sequences. The Priabonian evaporites are characterized by the presence of banded halite, by rhythmic potash facies (sylvite, carnallite), and by fine preservation of primary crystalline fabrics with no evidence of exposure. Their marine origin is well established by geochemical and isotopic criteria (Ortí, 1997).

In the Navarra basin, the evaporite sequence (fig. 6) consists of a layer of basal anhydrite (~1 m) above marine marls, followed by a Lower Halite Unit (LHU, 20 m), a potash zone consisting of sylvite beds (2 m) and carnallite beds (10 m), and an Upper Halite Unit (UHU, 40 m). The sequence is overlain by sabkha sediments consisting of clay minerals with anhydrite nodules (Ayora, Garçia-Veigas, and Pueyo, 1994a). The bromine content in the Navarra Basin halite rises from 50 ppm at the bottom of the Lower Halite Unit to 150 ppm close to the potash zone, which agrees well with the bromine concentrations expected during halite precipitation from evaporated seawa-

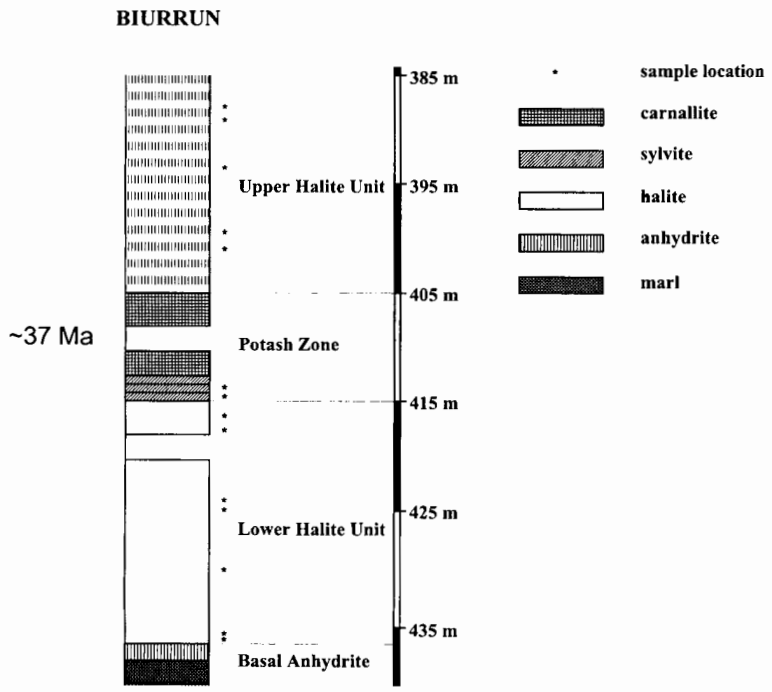

Fig. 6. Section through the Biurrun borehole of the Eocene Navarra Basin in Spain indicating the positions of halite sampling. Simplified after Ayora, Garçia-Veigas, and Pueyo (1994a).

ter. No evidence of exposure or very shallow water conditions were reported for the Lower and Upper Halite Unit (Ayora, Garçia-Veigas, and Pueyo, 1994a).

Aggregates of hopper crystals with fluid inclusions of primary origin are abundant in the bottom part of the Lower Halite Unit. They are extremely scarce or absent within the top 4 m of the Lower Halite Unit and within the Upper Halite Unit, where accumulations of platy halite crystals are observed (Ayora, Garçia-Veigas, and Pueyo, 1994a). The sylvite zone of the Biurrun borehole consists of a red horizon with alternating bands of halite and anhydrite; the halite crystals are rounded and cemented by sylvite. The Sylvite Member (2 m) in the Subiza mine consists of alternating centimeter-thick layers of halite and sylvite and millimeter-thick layers of dark clays and polyhalite (Cendón, Ayora, and Pueyo, 1998). The Carnallite Member (10 m) contains alternating beds of coarse-grained, usually brecciated reddish carnallite and thinner halite, anhydrite, and clay horizons.

Primary fluid inclusions were studied in 14 halite samples (Ayora, Garçia-Veigas, and Pueyo, 1994a) from the Biurrun borehole and in 6 samples from a section of the Subiza mine, 1 km north of Biurrun (table 1). Seven samples are from the Lower Halite Unit of the Biurrun borehole, 2 from the potash zone, and 5 from the Upper Halite Unit (fig. 6). In the Subiza mine 4 samples are from the Lower Halite Unit; 2 are from the potash zone (although it is not clear from which part). Based on the stratigraphy and on sedimentological evidence, the most promising section to find inclusions of evaporated seawater prior to potash facies is in the lowest section of the Biurrun borehole (samples BI-437 to BI-425).

TABLE 1

Major species concentrations and Jänecke units of fluid inclusions in Eocene marine halite from the Navarra Basin in Spain. Data set from Ayora, Garçia-Veigas, and Pueyo (1994a)

	sample		stratigraphy	method	Na	K	Mg	Ca	Cl	SO_4	CB	Mg	2K	SO_4	H_2O	2NaCl
					mmol/kg H_2O							Jänecke units				
	mSW (Bruland, 1983)				485	11	55	11	566	29	0.5	69.0	6.5	24.5	70215	307
	BI-388	p	upper halite	EDS-SEM	1170	120	3180	0	7610	70	-1.3	96.1	1.8	2.1	1677	17.7
	BI-389	p	upper halite	EDS-SEM	1870	120	2440	0	7260	70	-7.4	94.9	2.3	2.7	2160	36.4
	BI-392	p	upper halite	EDS-SEM	1460	160	2810	0	7520	50	-5.1	95.6	2.7	1.7	1888	24.8
	BI-397	p	upper halite	EDS-SEM	1710	180	2650	0	7150	80	-1.7	94.0	3.2	2.8	1968	30.3
	BI-399	p	upper halite	EDS-SEM	1550	150	2680	0	7510	20	-6.7	96.6	2.7	0.7	2000	27.9
	BI-414	p	potash	EDS-SEM	1310	430	2890	0	7910	140	-8.5	89.1	6.6	4.3	1711	20.2
	BI-415	p	potash	EDS-SEM	1730	620	2430	0	7750	120	-10.3	85.0	10.8	4.2	1941	30.2
	BI-417	p	lower halite	EDS-SEM	1690	400	2440	0	6750	200	-2.5	85.9	7.0	7.0	1955	29.8
	BI-419	p	lower halite	EDS-SEM	1650	580	2430	0	7170	160	-5.5	84.4	10.1	5.6	1927	28.6
	BI-424	p	lower halite	EDS-SEM	1890	480	2340	0	6960	160	-3.2	85.4	8.8	5.8	2026	34.5
sw	BI-425	ch	lower halite	EDS-SEM	2640	560	1870	0	6570	160	0.7	81.0	12.1	6.9	2403	57.1
sw	BI-430	ch	lower halite	EDS-SEM	2580	520	1650	0	6640	120	-7.2	81.3	12.8	5.9	2734	63.5
sw	BI-436	ch	lower halite	EDS-SEM	2730	400	1690	0	6590	150	-5.7	82.8	9.8	7.4	2721	66.9
sw	BI-437	ch	lower halite	EDS-SEM	3680	360	1360	0	6910	140	-6.2	81.0	10.7	8.3	3304	110
	SUB-30	p	potash	EDS-SEM	1270	590	2960	0	7700	160	-3.0	86.7	8.6	4.7	1625	18.6
	SUB-25	p	potash	EDS-SEM	1250	530	2950	0	7490	130	-0.9	88.2	7.9	3.9	1659	18.7
	SUB-11	p	lower halite	EDS-SEM	1110	760	3060	0	7970	160	-3.7	85.0	10.6	4.4	1542	15.4
	SUB-06	p	lower halite	EDS-SEM	1440	740	2810	0	7460	150	0.5	84.4	11.1	4.5	1667	21.6
	SUB-03	p	lower halite	EDS-SEM	1530	760	2440	0	7450	150	-7.8	82.2	12.8	5.1	1869	25.8
	SUB-01	p	lower halite	EDS-SEM	1330	960	2860	0	7640	190	-0.1	81.0	13.6	5.4	1572	18.8

sw: evaporated seawater prior to potash facies (screening based on $DE_{ELEMENT}$ pattern)
p: primary sedimentation in evaporite basin
ch: hopper crystals or chevrons
CB: charge balance
mSW: modern seawater
Comment: Only primary fluid inclusions in chevron halite were considered for $DE_{ELEMENT}$ screening.

All the compositions of primary fluid inclusions of the Eocene marine halites plot in the stability fields of sylvite and carnallite (fig. 7). The values of DE_K between 70 and 90 for primary fluid inclusions in the Lower Halite Unit of Subiza (SUB-01 to SUB-11, table 2) clearly indicate that these brines do not represent seawater prior to potash mineral precipitation. The $DE_{ELEMENT}$ pattern of primary fluid inclusions in the bottom sample SUB-01 ($DE_K = 91$, $DE_{MG} = 52$; table 2) is close to that of evaporated, in magnesium and sulfate depleted seawater near the beginning of sylvite precipitation ($DE_K = 90$, $DE_{MG} = 60$; Zimmermann, 2000a). The $m(H_2O)$-value of 1572 and the 2NaCl-value of 18.8 in sample SUB-01 (table 1) are also close to the values of 1370 and 17, which are expected for evaporated, KCl-saturated and in $MgSO_4$ depleted seawater.

The decrease in DE_K from 91 to 50 of inclusion fluids toward the potash zone and their nearly constant DE_{MG} of 52 (SUB-03 to SUB-11; table 2) are consistent with a shift in DE_K from 90 to 60 and a constant value of DE_{MG} around 60 predicted for the precipitation of sylvite during the evaporation of seawater depleted in $MgSO_4$ (Zimmermann, 2000a). The decrease in $m(H_2O)$-values from 1869 to 1542 and in 2NaCl-values from 25.8 to 15.4 of the fluid inclusions toward the top of the lower halite of the Subiza mine (SUB-03 to SUB-11) also reflects a progressive evaporation trend. The compositions of these primary fluid inclusions, plotted in the Jänecke diagram at 25 °C (fig. 7), move away from the dolomitization path along a straight line toward Q, which is expected while sylvite precipitates prior to the crystallization of carnallite. Although there is considerable evidence that the primary inclusion brines in samples SUB01 to

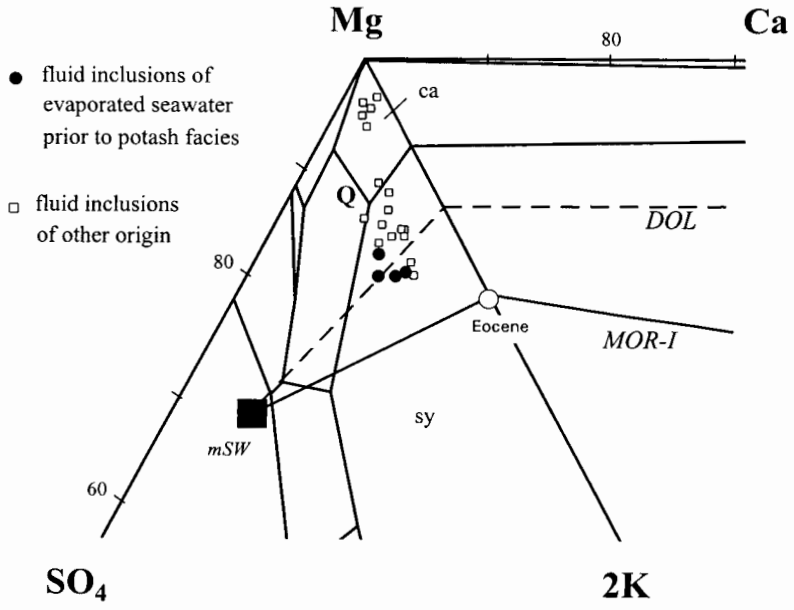

Fig. 7. Compositions of primary fluid inclusions (unfilled squares) in Eocene marine halites from the Navarra Basin (Spain) in the Jänecke plot of the NaCl-KCl-Na_2SO_4-$MgCl_2$-$CaCl_2$-H_2O system at 25°C. Fluid inclusions that fit the $DE_{ELEMENT}$ pattern of evaporated, Mg-depleted seawater prior to potash facies are marked as black filled circles.

mSW = plotting point of modern seawater, black filled square; *MOR-I* = predicted seawater chemistry for variations in sea floor spreading rates according to Hardie (1996 and personal communication), unfilled circle marks composition proposed for Eocene seawater; *DOL* = predicted chemistry of seawater affected by the dolomitization of limestones during evaporative concentration. ca = stability field of carnallite, sy = stability field of sylvite, Q = invariant brine composition in Jänecke plot (for labeling see e.g., Braitsch, 1962; Usdowski and Dietzel, 1998).

SUB 11 originate from the evaporative concentration of seawater during the precipitation of sylvite, bromine concentrations are necessary to prove unambiguously that the brines have not been affected by the dissolution of potash minerals. In any case, the primary fluid inclusions of the lower halite of the Subiza mine do not contain simply evaporated seawater prior to potash facies. Therefore they cannot be used to constrain the initial composition of seawater in the Navarra Basin.

The compositions of primary fluid inclusions in the upper section of the lower halite (platy crystals, BI-424 to BI-417) and in the potash zone from Biurrun (BI-415 to BI-414) are almost identical to the brines trapped within the potash zone of Subiza (SUB-25, SUB-30) except that they have comparatively higher m(H_2O)-values around 2000 and 2 NaCl-values around 30 (tables 1 and 2). The higher values in these primary fluid inclusions suggest the recycling of evaporites during the deposition of the potash zone in the sedimentary basin. This interpretation is in agreement with the mineralogy of the potash zone in Biurrun, which consists of rounded halite crystals that are cemented by sylvite.

The primary fluid inclusions trapped in the Upper Halite Unit above the potash zone of Biurrun (BI-399 to BI-388) are very different from the fluids of the Lower Halite Unit and within the potash beds. Their DE_K values between 11 and 17 (table 2) are within the typical range of evaporated seawater at the beginning of halite precipitation. However, their DE_{MG}/DE_K–ratios between 2.8 and 5.1 instead of ≤ 1 indicate that they are not evaporated in magnesium depleted seawater prior to potash

TABLE 2

$DE_{ELEMENT}$ patterns of fluid inclusions in Eocene marine halite from the Navarra Basin in Spain. Data set from Ayora, Garçia-Veigas, and Pueyo (1994a)

	sample		stratigraphy	DE_{MG}	DE_{K}	DE_{MG}/DE_{K}
	BI-388	p	upper halite	57.6	11.3	5.08
	BI-389	p	upper halite	44.2	11.3	3.90
	BI-392	p	upper halite	50.9	15.1	3.37
	BI-397	p	upper halite	48.0	17.0	2.82
	BI-399	p	upper halite	48.6	14.2	3.42
	BI-414	p	potash	52.4	40.7	1.29
	BI-415	p	potash	44.0	58.6	0.75
	BI-417	p	lower halite	44.2	37.8	1.17
	BI-419	p	lower halite	44.0	54.8	0.80
	BI-424	p	lower halite	42.4	45.4	0.93
sw	BI-425	ch	lower halite	33.9	53.0	0.64
sw	BI-430	ch	lower halite	29.9	49.2	0.61
sw	BI-436	ch	lower halite	30.6	37.8	0.81
sw	BI-437	ch	lower halite	24.7	34.0	0.72
	SUB-30	p	potash	53.7	55.8	0.96
	SUB-25	p	potash	53.5	50.1	1.07
	SUB-11	p	lower halite	55.5	71.9	0.77
	SUB-06	p	lower halite	50.9	70.0	0.73
	SUB-03	p	lower halite	44.2	71.9	0.62
	SUB-01	p	lower halite	51.8	90.8	0.57

sw: evaporated seawater prior to potash facies (screening based on $DE_{ELEMENT}$ pattern)
p: primary sedimentation in evaporite basin
ch: hopper crystals or chevrons
DE: degree of evaporation
Comment: only primary fluid inclusions in chevron halite were considered for $DE_{ELEMENT}$ screening

facies (Zimmermann, 2000a). The average Jänecke units of these samples are 95.4 ± 0.9 mole percent for Mg, 2.5 ± 0.5 mole percent for 2K, and 2.0 ± 0.8 mole percent for SO_4. They plot in the carnallite field (fig. 7), but most of their $m(H_2O)$-values around 2000 are higher than the $m(H_2O)$-values between 900 and 1300 expected for carnallite-saturated brines in the NaCl-KCl-$MgCl_2$-Na_2SO_4-H_2O system at 25 °C. The 2NaCl-values of the inclusion fluids in the range of 17.7 to 36.4 are also significantly higher than the predicted 2NaCl-values for carnallite saturated brines of 6 to 0.6. These primary fluid inclusions were most likely trapped in halite, which precipitated during the dissolution of initially deposited carnallite (or even bischofite) beds by the influx of

more dilute, halite-saturated seawater into the evaporite basin. Although primary in origin these fluid inclusions cannot be used for the reconstruction of the composition of Eocene seawater.

Only the primary fluid inclusions in chevron halite of samples BI-437 to BI-425 from the bottom of the Lower Halite Unit in Biurrun contain brines that fit the $DE_{ELEMENT}$ pattern for simply evaporated, in magnesium depleted seawater prior to potash facies (Zimmermann, 2000a). Their DE_K between 34 to 53 are below 60 with DE_{MG}/DE_K–ratios ≤ 1 (table 2). These fluid inclusions are marked as filled black circles in the Jänecke diagram and plot next to the dashed line, which represents the path of seawater affected by the dolomitization of limestones (*DOL*, fig. 7). Their average Jänecke units are 81.5 ± 0.7 mole percent for Mg, 1.4 ± 1.2 mole percent for 2K, and 7.1 ± 0.9 mole percent for SO_4. Decreasing $m(H_2O)$-values from 3304 to 2403 and decreasing 2NaCl-values from 110 to 57 for samples BI-437 to BI-425 (table 1) indicate saturation of these brines with halite but not with sylvite ($m(H_2O) \leq 1370$, $2NaCl \leq 17$; Zimmermann, 2000a). They also suggest progressive evaporation within the profile. With further evaporation these inclusion brines would precipitate sylvite, followed by carnallite, which is consistent with the mineralogy of the potash beds of the Navarra Basin.

Oligocene

The Mulhouse Basin (fig. 4) is part of the European intracontinental rift system (Sissingh, 1998). It is filled with an Upper Eocene to Lower Oligocene evaporite sequence, which is 1600 m thick. The evaporites were deposited on top of post-rift continental mudstones and conglomerates and were covered by Rupelian marine sediments (Blanc-Valleron and Schuler, 1997). The main evaporitic sequence has been subdivided into three formations (Lower, Middle, and Upper Salt formations). At the base of the Upper Salt (Salt IV member) they include two sylvite seams, whose average thickness is 2 to 4 m and which are separated by about 20 m of alternating halite and marls (Blanc-Valleron, 1991; Hofmann and others, 1993).

The marine origin of the evaporite sequence in the Rhine Graben has been questioned by Fontes and others (1991), who based on isotopic studies suggested that they are precipitates of redissolved salt of Permo-Triassic origin within a closed hydrological system. However, there is strong paleontological, sedimentological, and geochemical evidence of marine influx during the deposition of at least the upper Middle and Upper Salt Formation (Blanc-Valleron and Schuler, 1997).

The presence of marine nannoplankton, shallow water benthic foraminifera, and well diversified dinokyste assemblages (Schuler 1988/90) in the marls immediately below the Salt IV member (Fossiliferous Zone) indicate marine influx. There seems no evidence of major hydrothermal input to the basin (B. C. Schreiber, personal communication). The composition of brines associated with these evaporites fall on the evaporation pathway of marine waters (Poutoukis, 1991). The bromine profile of halite from the base of the Salt IV (70 μg Br/g halite) up to the top of the lower potash seam (320μg Br/g halite) corresponds with the progressive concentration of seawater (Baar and Kühn, 1962; Kühn and Roth, 1979). The halite within the sequence shows remarkable preservation of primary depositional textures. Chevrons with competitive growth textures and cumulates of hopper crystals are well preserved and indicate subaqueous deposition at shallow water depths; there is no evidence for subaeral exposure (Lowenstein and Spencer, 1990).

Classically the potash salts and associated sediments are interpreted as primary. The two sylvite seams are well bedded and consist of laminar mudstone, anhydrite, halite, and sylvite forming centimeter- to decimeter-scale mineralogical cycles, which are present in lateral continuity throughout the entire basin. The bromine concentrations of 2600 μg Br/g sylvite and 260 μg Br/g halite (10:1) in sylvinitic rocks and of

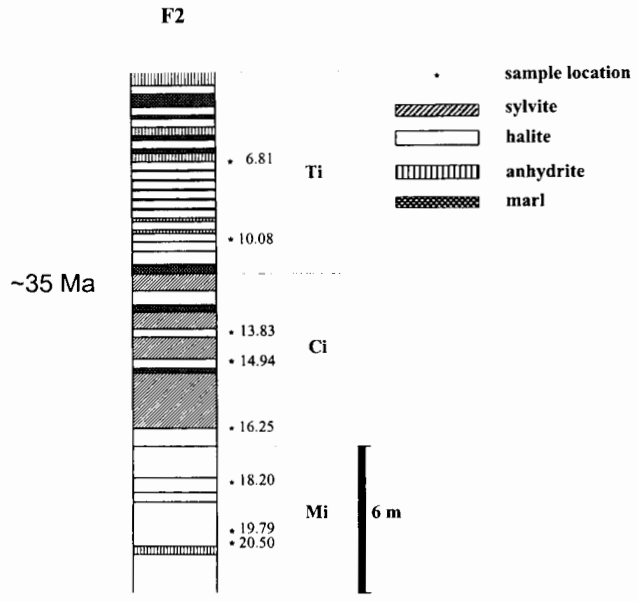

Fig. 8. Section through the F2 borehole of the Oligocene Mulhouse Basin in France indicating the positions of halite sampling. Simplified after Canals, Carpentier, Huc, and others (1993).

2830 μg Br/g carnallite, 3320 μg Br/g sylvite, and 380 μg Br/g halite (7:9:1) in carnallitic rocks indicate their crystallization from evaporated seawater (Braitsch and Herrmann, 1964). There is evidence that the sylvite crystallized during the cooling of these brines (Braitsch and Herrmann, 1964; Lowenstein and Spencer, 1990).

Eight halite samples were taken from the upper part of the evaporitic series in borehole F2 (fig. 8). The drill core passes through a 20 m section of Salt IV, which consists of 10 to 20 m of halite beds and 5 m of anhydrite/marl beds (Canals and others, 1993; Hofmann and others, 1993). The halite beds contain 10 cm-thick cycles of halite with laminations of dolomitic marls and anhydrite. Some of the halite beds contain sylvite. The section from bottom to top is divided into subunits Mi (6 m), Ci (5.5 m), and Ti (6 m). Subunit Mi consists of halite intercalated with marl layers and one anhydrite horizon. Sample 20.50 (sample numbers indicate depth in meters of profile) was collected just above this anhydrite layer, sample 19.79 from the middle part of the halite bed (fig. 8). Subunit Ci consists of halite layers interbedded with sylvite horizons. Sample 16.25 was taken from the bottom of Ci within the halite bed below the first sylvite bed (1-2 m); sample 14.94 was collected from the bottom part of the halite bed above this first sylvite bed (fig. 8). Sample 13.83 was taken from the halite bed above the second sylvite bed (<1 m). Subunit Ti contains alternating layers of halite, dolomitic marl, and anhydrite. Sample 10.08 was collected from the lower *third of* this subunit, sample 6.81 from the topmost part. Canals and others (1993) took special care to analyze only primary fluid inclusions in halite with chevron textures. The stratigraphy suggests that samples 20.50 and 19.79 from the lowest section of the F2 borehole are the most promising for reconstructing the chemistry of seawater in the Oligocene Mulhouse Basin.

According to Canals and others (1993) fluid inclusions in samples 18.20 and 13.83 are not saturated with halite, and sample 16.25 shows a charge balance of –30.8 percent (table 3). The analyses of these 3 samples were therefore rejected. The compositions of the primary fluid inclusions in the remaining 5 Oligocene marine halite samples plot

in the stability fields of sylvite and carnallite (fig. 9). The fluid inclusions of 3 halite samples are $MgSO_4$-free and contain small quantities of $CaCl_2$. They plot in the Mg-Ca-2K part of the Jänecke diagram (fig. 9).

TABLE 3

Major species concentrations and Jänecke units of fluid inclusions in Oligocene marine halite from the Mulhouse Basin in France. Data set from Canals and others (1993)

	sample		stratigraphy	method	Na	K	Mg	Ca	Cl	SO	CB	Mg	2K	SO_4	Ca	H_2O	2NaCl
					mmol/kg H_2O							Jänecke units					
	6.81	ch	Salt IV	LA-ICPAES, EDS-SEM	1097	394	3285	227	7546	38	11.1	89.5	5.4		5.2	1512	14.9
	10.08	ch	Salt IV	LA-ICPAES, EDS-SEM	767	263	4111		9492	54	-3.7	95.7	3.1	1.2		1292	8.9
	13.83	ch	Salt IV	LA-ICPAES, EDS-SEM	832	261	1993		5501	20	-8.7	not saturated with halite					
	14.94	ch	Salt IV	LA-ICPAES, EDS-SEM	1034	679	2761	112	7609	64	-3.7	87.7	10.8		1.5	1763	16.4
	16.25	ch	Salt IV	LA-ICPAES, EDS-SEM	1217	680	2015	49	8050	84	-30.8	see charge balance					
	18.20	ch	Salt IV	LA-ICPAES, EDS-SEM	2022	594	1169		5280	59	-8.6	not saturated with halite					
sw	19.79	ch	Salt IV	LA-ICPAES, EDS-SEM	2280	481	1604	117	6370	36	-3.8	83.3	12.5		4.2	2883	59
sw	20.50	ch	Salt IV	LA-ICPAES, EDS-SEM	3024	369	1187	43	5402	60	5.8	85.5	13.3	1.3		3995	109

sw: evaporated seawater prior to potash facies (screening based on $DE_{ELEMENT}$ pattern)
ch: hopper crystals or chevrons
CB: charge balance

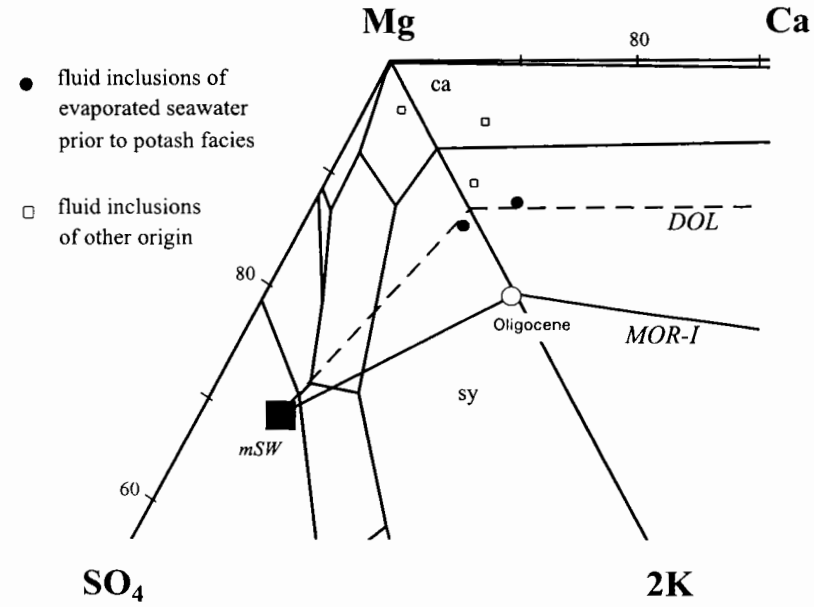

Fig. 9. Compositions of primary fluid inclusions (unfilled squares) in Oligocene marine halites from the Mulhouse Basin (France) in the Jänecke plot of the NaCl-KCl-Na_2SO_4-$MgCl_2$-$CaCl_2$-H_2O system at 25°C. Fluid inclusions that fit the $DE_{ELEMENT}$ pattern of evaporated, Mg-depleted seawater prior to potash facies are marked as black filled circles.

mSW = plotting point of modern seawater, black filled square; *MOR-I* = predicted seawater chemistry for variations in sea floor spreading rates according to Hardie (1996 and personal communication), unfilled circle marks composition proposed for Oligocene seawater; *DOL* = predicted chemistry of seawater affected by the dolomitization of limestones during evaporative concentration. ca= stability field of carnallite, sy=stability field of sylvite.

TABLE 4

$DE_{ELEMENT}$ patterns of fluid inclusions in Oligocene marine halite from the Mulhouse Basin in France. Data set from Canals and others (1993)

	sample	stratigraphy	DE_{MG}	DE_K	DE_{MG}/DE_K
	6.81 ch	Salt IV	59.5	37.3	1.60
	10.08 ch	Salt IV	74.5	24.9	3.00
	13.83 ch	Salt IV	not saturated with halite		
	14.94 ch	Salt IV	50.0	64.2	0.78
	16.25 ch	Salt IV	see charge balance		
	18.20 ch	Salt IV	not saturated with halite		
sw	19.79 ch	Salt IV	29.1	45.5	0.64
sw	20.50 ch	Salt IV	21.5	34.9	0.62

sw: evaporated seawater prior to potash facies (screening based on $DE_{ELEMENT}$ pattern)
ch: hopper crystals or chevrons
DE: degree of evaporation

The $DE_{ELEMENT}$ patterns of the primary fluid inclusions in samples 6.81 and 10.08 from the upper part of the section with DE_{MG}=75-60, DE_K=25-37, and DE_{MG}/DE_K-ratios of 1.5 and 3.0 (table 4) do not fit the criteria for evaporated, in magnesium depleted seawater prior to potash facies. The fluid inclusion compositions of both samples plot in the stability field of carnallite. Their m(H_2O)-values of 1512 and 1292 are close to the value of 1310, which is expected for saturation with respect to carnallite; their 2NaCl-values of 14.9 and 8.9 are slightly higher than the expected value of 6. Thus, it seems likely that the primary fluid inclusions in this part of the evaporite sequence reflect progressively concentrated brines saturated with carnallite, rather than products of recycled potash minerals. In any case, they cannot be used for the reconstruction of the composition of unevaporated seawater in the Oligocene basin.

The composition of primary fluid inclusions in halite sample 16.25 with a DE_K of 64.3 (table 4) cannot be used to constrain the composition of unevaporated seawater in the sedimentary basin. It plots within the stability field of sylvite. The inclusion brine is saturated with sylvite, which is indicated by its m(H_2O)-value of 1763 as compared to 1550 and its 2 NaCl-value of 16.4 compared to 20 for the beginning of sylvite precipitation (Zimmermann, 2000a).

Only the primary fluid inclusions in samples 19.79 and 20.50 from below the sylvite seams fit the $DE_{ELEMENT}$ pattern of evaporated and in magnesium depleted seawater prior to potash facies. Their DE_K values of 35 and 46 are clearly below 60, and they show DE_{MG}/DE_K-ratios $\leq$1 (table 4). Their compositions are marked as black filled circles in the Jänecke diagram and plot close to the dolomitization path of seawater affected by the dolomitization of limestones (*DOL*, fig. 9). The m(H_2O)-values of 3995 and 2883 and 2NaCl-values of 109 and 59 (table 3) indicate that the fluid inclusions in the two basal halite samples, 20.50 and 19.79, are saturated with halite but not with sylvite (m(H_2O) $\leq$1550, 2NaCl $\leq$20). These inclusions seem to contain evaporated seawater (depleted in Mg) prior to potash mineral precipitation. If evaporated further sylvite followed by carnallite would precipitate from these brines. This is consistent with the mineralogy of the potash beds in the Mulhouse Basin.

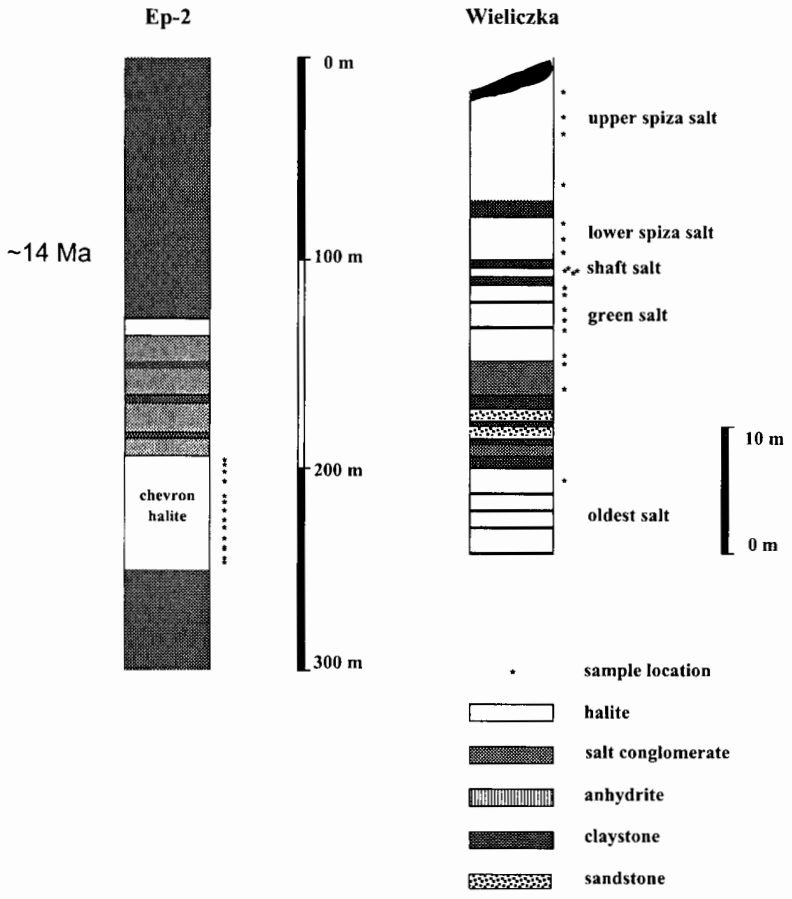

Fig. 10. Sections through the Badenian evaporites of the Ep-2 borehole in the East Slovakian Basin and of the Wieliczka mine in the Forecarpathian Basin in Eastern Europe indicating the positions of halite sampling. Simplified after Galamay and Karoli (1997) and Galamay, Bukowski, and Przybylo (1997).

Lower-Middle Miocene (Badenian)

The Miocene evaporites of the Carpathian region (fig. 4) were deposited in the Forecarpathian Basin and in several intermontane depressions (East Slovakian Basin, Transcarpathian Basin, Transylvanian Basin) spread over Slovakia, Poland, Ukraine, and Romania (Kovalevich and Petrichenko, 1997). These evaporites have an age of 14 Ma (Badenian) to 22 Ma (Eggenburgian). Their marine origin is confirmed by isotopic evidence and by the bromine distribution in halite (Garlicki and Wiewiórka, 1981; Garçia Veigas, Rossel, and Garlicki, 1997; Peryt and others, 1997). Peryt and others (1997) report $\delta^{18}O$ SMOW values of $+12.9 \pm 0.5$ permil and $\delta^{34}S$ CDT values of 22.7 ± 0.4 permil for Badenian gypsum, which are characteristic of Tertiary sulfates of marine origin (Claypool and others, 1980). Galamay and Karoli (1997) report bromine concentrations in basal chevron halite between 40 and 89 ppm for the East Slovakian Basin, the average bromine content is 55 ppm, which is consistent with bromine concentrations in the first halite, which precipitates from evaporated seawater.

Kovalevich and Petrichenko (1997) report fluid inclusion analyses by the Petrichenko method of 23 halite samples of Badenian, Karpatian, and Eggenburgian age

TABLE 5

Major species concentrations and Jänecke units of fluid inclusions in Badenian marine halite from the Carpathian region in Eastern Europe. Data sets from Kovalevich and Petrichenko (1997), Galamay and Karoli (1997), Galamay, Bukowski, and Przybylo (1997), and Garçia Veigas, Rossel, and Garlicki (1997)

	Basin	formation		sample	method	Na	K	Mg	Ca	Cl	SO_4	CB	Mg	2K	SO_4	H_2O	2NaCl
						mmol/kg H_2O							Jänecke units				
	KOVALEVIC AND PETRICHENKO (1997)																
sw	FCB (Poland)	Wieliczka	ch	breccia	PETRICHENKO	144	818				135.64		79.7	7.0	13.2	5692	
sw	FCB (Poland)	Wieliczka	ch	spiza salt	PETRICHENKO	155.3	918				183.91		77.8	6.6	15.6	6546	
sw	FCB (Poland)	Wieliczka	ch	spiza salt	PETRICHENKO	273.9	1195				193.11		78.4	9.0	12.7	8464	
sw	FCB (Poland)	Wieliczka	ch	shaft salt	PETRICHENKO	225.9	945				129.89		79.6	9.5	10.9	6593	
sw	FCB (Poland)	Wieliczka	ch	green salt	PETRICHENKO	262.6	877				201.15		72.5	10.9	16.6	6713	
	FCB (Ukraine)	Tyras		Sel.-St.-348	PETRICHENKO	299.4	1031				342.54		67.7	9.8	22.5	8457	
	FCB (Ukraine)	Tyras		Sel.-St.-348	PETRICHENKO	299.4	1404				281.62		76.5	8.2	15.3	10186	
	FCB (Ukraine)	Tyras		Zabolotiv	PETRICHENKO	409.5	1172				356.33		67.6	11.8	20.6	9621	
	FCB (Romania)			Slanic-Prah.	PETRICHENKO	172.3	900				185.06		76.8	7.4	15.8	6498	
	ESB	Zbudza	ch	Zb-1	PETRICHENKO	175.1	1036				118.39		83.4	7.1	9.5	6893	
	ESB	Zbudza	ch	Ep-2, 236.4	PETRICHENKO	124.3	800				134.49		80.3	6.2	13.5	5530	
sw	ESB	Zbudza	ch	Ep-2, 238.4	PETRICHENKO	152.5	804				160.92		77.2	7.3	15.5	5780	
sw	ESB	Zbudza	ch	Ep-2, 239.2	PETRICHENKO	146.9	786				157.48		77.3	7.2	15.5	5644	
	TCB (Ukraine)	Tereblin		Solotvyne	PETRICHENKO	437.7	1295				419.55		67.0	11.3	21.7	10731	
	TCB (Ukraine)	Tereblin		Mukacheve	PETRICHENKO	268.3	818				229.89		69.2	11.4	19.5	6560	
	TSB (Romania)			Victoria P04	PETRICHENKO	254.2	927				198.86		74.0	10.1	15.9	6954	
	TSB (Romania)			Victoria P11	PETRICHENKO	262.6	645				80.462		75.3	15.3	9.4	4756	
	TSB (Romania)			Victoria P12	PETRICHENKO	276.8	1127				339.09		70.2	8.6	21.1	8904	
	TSB, Romania			O. Dej P50	PETRICHENKO	192	618				94.255		76.5	11.9	11.7	4486	
	GALAMAY AND KAROLI (1997)																
sw	ESB	Zbudza	ch	Ep-2, 71	PETRICHENKO	144	631				100		78.6	9.0	12.4	4460	
sw	ESB	Zbudza	ch	Ep-2, 70	PETRICHENKO	135.6	609				101.15		78.3	8.7	13.0	4317	
sw	ESB	Zbudza	ch	Ep-2, 68	PETRICHENKO	110.1	591				97.704		79.4	7.4	13.1	4126	
sw	ESB	Zbudza	ch	Ep-2, 65	PETRICHENKO	155.3	759				104.6		80.6	8.3	11.1	5223	
sw	ESB	Zbudza	ch	Ep-2, 63	PETRICHENKO	146.9	586				108.05		76.4	9.6	14.1	4260	
sw	ESB	Zbudza	ch	Ep-2, 61	PETRICHENKO	127.1	518				95.405		76.5	9.4	14.1	3757	
sw	ESB	Zbudza	ch	Ep-2, 59	PETRICHENKO	121.4	613				98.853		79.4	7.9	12.8	4290	
sw	ESB	Zbudza	ch	Ep-2, 57	PETRICHENKO	135.6	581				103.45		77.3	9.0	13.7	4178	
sw	ESB	Zbudza	ch	Ep-2, 56	PETRICHENKO	144	563				101.15		76.5	9.8	13.7	4088	
sw	ESB	Zbudza	ch	Ep-2, 55	PETRICHENKO	146.9	591				112.65		76.0	9.5	14.5	4311	
sw	ESB	Zbudza	ch	Ep-2, 54	PETRICHENKO	132.7	550				98.853		76.9	9.3	13.8	3968	
sw	ESB	Zbudza	ch	Ep-2, 53	PETRICHENKO	127.1	604				111.5		77.5	8.2	14.3	4326	
sw	ESB	Zbudza	ch	Ep-2, 52	PETRICHENKO	127.1	572				110.35		76.7	8.5	14.8	4143	
sw	ESB	Zbudza	ch	Ep-2, 50	PETRICHENKO	93.2	500				94.255		78.0	7.3	14.7	3556	

GALAMAY AND OTHERS (1997)																	
sw	FCB (Poland)	Wieliczka	ch	105	PETRICHENKO		172.3	813		159.77		76.8	8.1	15.1	5879	
sw	FCB (Poland)	Wieliczka	ch	106	PETRICHENKO		169.4	804		122.99		79.5	8.4	12.2	5617	
sw	FCB (Poland)	Wieliczka	ch	107	PETRICHENKO		155.3	809		118.39		80.5	7.7	11.8	5577	
sw	FCB (Poland)	Wieliczka	ch	16	PETRICHENKO		183.6	863		137.93		79.0	8.4	12.6	6067	
sw	FCB (Poland)	Wieliczka	ch	120	PETRICHENKO		169.4	909		116.09		81.9	7.6	10.5	6158	
sw	FCB (Poland)	Wieliczka	ch	118	PETRICHENKO		217.5	890		140.23		78.1	9.5	12.3	6325	
sw	FCB (Poland)	Wieliczka	ch	117	PETRICHENKO		206	904		117		80.4	9.2	10.4	6241	
sw	FCB (Poland)	Wieliczka	ch	98	PETRICHENKO		212	850		118		79.1	9.9	11.0	5961	
sw	FCB (Poland)	Wieliczka	ch	100	PETRICHENKO		211.8	850		128.74		78.4	9.8	11.9	6018	
sw	FCB (Poland)	Wieliczka	ch	99	PETRICHENKO		155.3	827		127.59		80.1	7.5	12.4	5729	
	FCB (Poland)	Wieliczka	ch	97	PETRICHENKO		121.4	750		121.84		80.4	6.5	13.1	5174	
sw	FCB (Poland)	Wieliczka	ch	6	PETRICHENKO		146.9	804		147.13		78.5	7.2	14.4	5688	
sw	FCB (Poland)	Wieliczka	ch	87	PETRICHENKO		146.9	854		131.04		80.7	6.9	12.4	5876	
sw	FCB (Poland)	Wieliczka	ch	91	PETRICHENKO		209	1013		131.04		81.1	8.4	10.5	6931	
sw	FCB (Poland)	Wieliczka	ch	89	PETRICHENKO		206	1022		143		80.6	8.1	11.2	7037	
sw	FCB (Poland)	Wieliczka	ch	12	PETRICHENKO		146.9	854		133.34		80.5	6.9	12.6	5889	
sw	FCB (Poland)	Wieliczka	ch	10	PETRICHENKO		158.1	909		142.53		80.4	7.0	12.6	6274	
	FCB (Poland)	Wieliczka	ch	9	PETRICHENKO		132.7	922		127.59		82.6	5.9	11.4	6196	
	FCB (Poland)	Wieliczka	ch	8	PETRICHENKO		127.1	859		139.08		80.9	6.0	13.1	5891	
sw	FCB (Poland)	Wieliczka	ch	20	PETRICHENKO		138.4	772		151.73		77.8	7.0	15.3	5513	
GARCIA VEIGAS AND OTHERS (1997)																	
	FCB (Poland)	Lezkowice Z-1	ch	1	EDS-SEM	4270	150	540	0	5460	140	-4.3	71.5	9.9	18.5	7352	283
	FCB (Poland)	Lezkowice Z-1	ch	7	EDS-SEM	4390	60	500	0	5500	120	-5.2	76.9	4.6	18.5	8540	338
	FCB (Poland)	Lezkowice Z-1	ch	8	EDS-SEM	4280	70	440	0	5520	120	-9.6	73.9	5.9	20.2	9329	360
	FCB (Poland)	Woszczyce IG1	ch	2	EDS-SEM	4140	130	570	0	5520	150	-7.3	72.6	8.3	19.1	7071	264
	FCB (Poland)	Woszczyce IG1	ch	4	EDS-SEM	4380	80	570	0	5570	140	-4.4	76.0	5.3	18.7	7401	292
	FCB (Poland)	Woszczyce IG1	ch	7	EDS-SEM	4300	70	440	0	5460	140	-8.9	71.5	5.7	22.8	9026	350

sw: evaporated seawater prior to potash facies (screening based on $DE_{ELEMENT}$ pattern)
ch: hopper crystals or chevrons
CB: charge balance
PETRICHENKO data in g/l. For transformation into mmol/kg H^2O a factor of 1.325 was used.

FCB Forecarpathian Basin
ESB East Slovakian Basin
TCB Transcarpathian Basin (Ukraine)
TSB Transylvanian Basin (Romania)

from the Carpathian region. They collected only a few samples from each site or subbasin and did not study complete stratigraphic sections. Their information regarding the stratigraphy and primary sedimentation textures in the individual samples is incomplete. Some of the fluid inclusions they analyzed were taken from halite, which reportedly did not contain primary textures or originated from salt domes. Therefore, this data set is poorly suited to constrain the composition of seawater during the Miocene. It is best to consider only their data for the East Slovakian Basin and the Forecarpathian Basin, which can be compared with the more detailed studies by Galamay, Bukowski, and Przybylo (1997) and Galamay and Karoli (1997).

Galamay and Karoli (1997) analyzed primary fluid inclusions in 14 chevron halite samples in the East Slovakian Basin from borehole Ep-2 (fig. 10) using the Petrichenko method. The maximum thickness of this evaporite sequence (Zbudza Formation) is 300 m; it consists predominantly of halite. Particularly in the lower part of the section in the bedded rock salt, which contains thin intercalations of anhydrite, chevrons crystals are common and well preserved. Kovalevich and Petrichenko (1997) also analyzed primary fluid inclusions in 4 halite samples of this formation.

Galamay, Bukowski, and Przybylo (1997) determined compositions of primary fluid inclusions in 20 halite samples with well preserved chevron crystals (up to 15 cm in length) from the Wieliczka mine (Forecarpathian Basin, Poland). Kovalevich and Petrichenko (1997) contributed data for 5 additional halite samples from the Wieliczka mine. In both studies the Petrichenko method was applied. The Forecarpathian Basin includes the detrital Skawina Beds (<500-800 m) that consist of marly mudstones, siltstones, and shales, and the marine evaporitic Wieliczka Beds (100-130 m) that contain halite and anhydrite. In detail the tectonic structure of this basin is very complicated. The samples cover a section of marine halite (25 m) that includes the stratiform green salts, the shaft salt, and the lower and upper spiza salt (fig. 10).

Garçia Veigas, Rossel, and Garlicki (1997) collected 6 fluid inclusion-bearing samples from the autochtonous rock salt section in the nearby Woszczyce IG1 and Lezkovice Z1 boreholes in the Forecarpathian Basin and analyzed the fluid inclusions by cryo-EDS-SEM. The compositions of the fluid inclusions in these samples are rather heterogeneous (tables 5 and 6). Garçia Veigas, Rossel, and Garlicki (1997) observed the rehydration of anhydrite to gypsum within the profiles. Recrystallization processes accompanying this rehydration may be responsible for the scatter in their data set. These analyses were not considered for evaluating the composition of Badenian seawater, although the study itself and especially the petrogaphic documentation were done very carefully.

Altogether, fluid inclusion data from 43 Badenian primary halite samples are considered in this review: 25 samples from the Forecarpathian Basin and 18 samples from the East Slovakian Basin. The compositions of the primary fluid inclusions in all Badenian halite samples fall in the stability field of kainite close to the boundary of the sylvite field (fig. 11).

The $DE_{ELEMENT}$ patterns of primary fluid inclusions in all 43 Badenian samples (Forcarpathian and Eastslovakian Basin) fit the predicted trend for evaporated (Mg-depleted) seawater prior to potash facies. The DE_K of the Forecarpathian samples varies between 12 and 20 (table 6); the DE_K of the fluid inclusions in the East Slovakian Basin ranges from 9 to 14 with DE_{MG}/DE_K-ratios close to 1. In the Jänecke diagram these inclusion brines are marked as gray filled circles for the Forecarpathian Basin and as black filled circles for the Eastslovakian Basin (fig. 11). The average compositions of both data sets from the Carpathian region plot close to the dashed line indicating the dolomitization path (*DOL*, fig. 11). The considerable scatter in the fluid inclusion compositions (see also tables 5 and 6) reflects the 20 percent uncertainty due to the imprecision of the Petrichenko method.

TABLE 6

$DE_{ELEMENT}$ patterns of fluid inclusions in Badenian marine halite from the Carpathian region in Eastern Europe. Data sets from Kovalevich and Petrichenko (1997), Galamay and Karoli (1997), Galamay, Bukowski, and Przybylo (1997), and Garçia Veigas, Rossel, and Garlicki (1997)

	Basin	formation		sample	DE_{MG}	DE_K	DE_{MG}/DE_K
	KOVALEVIC AND PETRICHENKO (1997)						
sw	FCB (Poland)	Wieliczka	ch	breccia	14.8	13.6	1.09
sw	FCB (Poland)	Wieliczka	ch	spiza salt	16.6	14.7	1.13
sw	FCB (Poland)	Wieliczka	ch	spiza salt	21.7	25.9	0.84
sw	FCB (Poland)	Wieliczka	ch	shaft salt	17.1	21.4	0.80
sw	FCB (Poland)	Wieliczka	ch	green salt	15.9	24.8	0.64
	FCB (Ukraine)	Tyras		Sel.-St.-348	18.7	28.3	0.66
	FCB (Ukraine)	Tyras		Sel.-St.-348	25.4	28.3	0.90
	FCB (Ukraine)	Tyras		Zabolotiv	21.2	38.7	0.55
	FCB (Romania)			Slanic-Prah.	16.3	16.3	1.00
	ESB	Zbudza	ch	Zb-1	18.8	16.6	1.13
	ESB	Zbudza	ch	Ep-2, 236.4	14.5	11.8	1.23
sw	ESB	Zbudza	ch	Ep-2, 238.4	14.6	14.4	1.01
sw	ESB	Zbudza	ch	Ep-2, 239.2	14.2	13.9	1.03
	TCB (Ukraine)	Tereblin		Solotvyne	23.5	41.4	0.57
	TCB (Ukraine)	Tereblin		Mukacheve	14.8	25.4	0.58
	TSB (Romania)			Victoria P04	16.8	24.0	0.70
	TSB (Romania)			Victoria P11	11.7	24.8	0.47
	TSB (Romania)			Victoria P12	20.4	26.2	0.78
	TSB, Romania			O. Dej P50	11.2	18.2	0.62
	GALAMAY AND KAROLI (1997)						
sw	ESB	Zbudza	ch	Ep-2, 71	11.4	13.6	0.84
sw	ESB	Zbudza	ch	Ep-2, 70	11.0	12.8	0.86
sw	ESB	Zbudza	ch	Ep-2, 68	10.7	10.4	1.03
sw	ESB	Zbudza	ch	Ep-2, 65	13.8	14.7	0.94
sw	ESB	Zbudza	ch	Ep-2, 63	10.6	13.9	0.76
sw	ESB	Zbudza	ch	Ep-2, 61	9.4	12.0	0.78
sw	ESB	Zbudza	ch	Ep-2, 59	11.1	11.5	0.97
sw	ESB	Zbudza	ch	Ep-2, 57	10.5	12.8	0.82
sw	ESB	Zbudza	ch	Ep-2, 56	10.2	13.6	0.75
sw	ESB	Zbudza	ch	Ep-2, 55	10.7	13.9	0.77
sw	ESB	Zbudza	ch	Ep-2, 54	10.0	12.6	0.79
sw	ESB	Zbudza	ch	Ep-2, 53	11.0	12.0	0.91
sw	ESB	Zbudza	ch	Ep-2, 52	10.4	12.0	0.86
sw	ESB	Zbudza	ch	Ep-2, 50	9.1	8.8	1.03

	Basin	formation		sample	DE_{MG}	DE_K	DE_{MG}/DE_K
	GALAMAY AND OTHERS (1997)						
sw	FCB (Poland)	Wieliczka	ch	105	14.7	16.3	0.90
sw	FCB (Poland)	Wieliczka	ch	106	14.6	16.0	0.91
sw	FCB (Poland)	Wieliczka	ch	107	14.7	14.7	1.00
sw	FCB (Poland)	Wieliczka	ch	16	15.6	17.4	0.90
sw	FCB (Poland)	Wieliczka	ch	120	16.5	16.0	1.03
sw	FCB (Poland)	Wieliczka	ch	118	16.1	20.6	0.78
sw	FCB (Poland)	Wieliczka	ch	117	16.4	19.5	0.84
sw	FCB (Poland)	Wieliczka	ch	98	15.4	20.0	0.77
sw	FCB (Poland)	Wieliczka	ch	100	15.4	20.0	0.77
sw	FCB (Poland)	Wieliczka	ch	99	15.0	14.7	1.02
	FCB (Poland)	Wieliczka	ch	97	13.6	11.5	1.18
sw	FCB (Poland)	Wieliczka	ch	6	14.6	13.9	1.05
sw	FCB (Poland)	Wieliczka	ch	87	15.5	13.9	1.11
sw	FCB (Poland)	Wieliczka	ch	91	18.4	19.8	0.93
sw	FCB (Poland)	Wieliczka	ch	89	18.5	19.5	0.95
sw	FCB (Poland)	Wieliczka	ch	12	15.5	13.9	1.11
sw	FCB (Poland)	Wieliczka	ch	10	16.5	15.0	1.10
	FCB (Poland)	Wieliczka	ch	9	16.7	12.6	1.33
	FCB (Poland)	Wieliczka	ch	8	15.6	12.0	1.30
sw	FCB (Poland)	Wieliczka	ch	20	14.0	13.1	1.07
	GARCIA VEIGAS AND OTHERS (1997)						
	FCB (Poland)	Lezkowice Z-1	ch	1	9.8	14.2	0.69
	FCB (Poland)	Lezkowice Z-1	ch	7	9.1	5.7	1.60
	FCB (Poland)	Lezkowice Z-1	ch	8	8.0	6.6	1.20
	FCB (Poland)	Woszczyce IG1	ch	2	10.3	12.3	0.84
	FCB (Poland)	Woszczyce IG1	ch	4	10.3	7.6	1.37
	FCB (Poland)	Woszczyce IG1	ch	7	8.0	6.6	1.20

sw: evaporated seawater prior to potash facies (screening based on $DE_{ELEMENT}$ pattern)
ch: hopper crystals or chevrons
DE: degree of evaporation

FCB Forecarpathian Basin
ESB East Slovakian Basin
TCB Transcarpathian Basin (Ukraine)
TSB Transylvanian Basin (Romania)

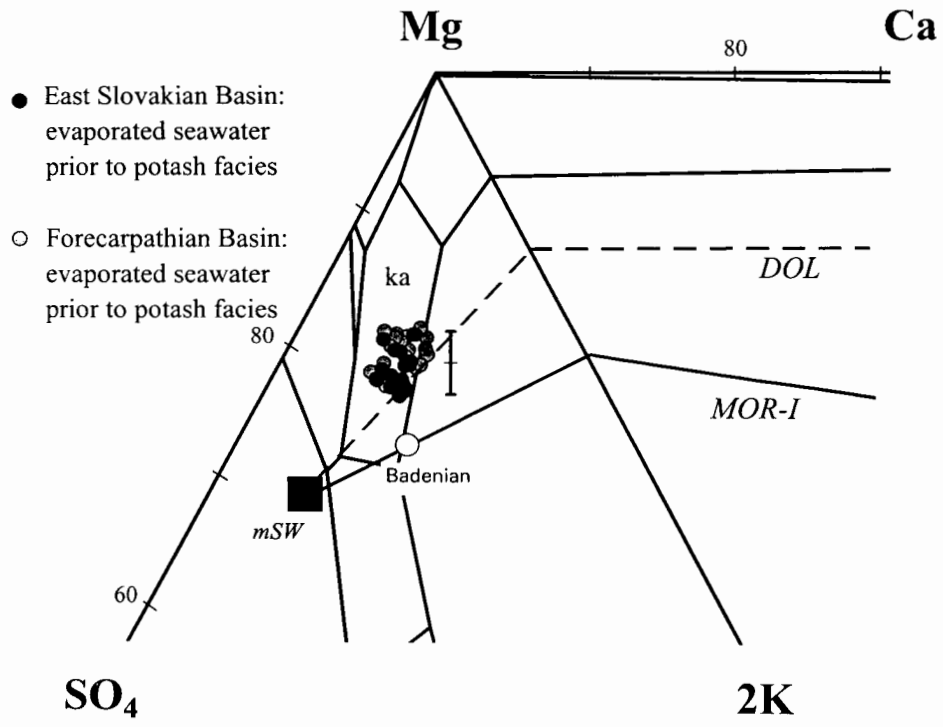

Fig. 11. Compositions of primary fluid inclusions in Badenian marine halites from the East Slovakian and Forecarpathian Basins (Eastern Europe) in the Jänecke plot of the NaCl-KCl-Na_2SO_4-$MgCl_2$-$CaCl_2$-H_2O system at 25°C. Fluid inclusions that fit the $DE_{ELEMENT}$ pattern of evaporated, Mg-depleted seawater prior to potash facies are marked as black or gray filled circles. The error bar indicates the analytical uncertainty of the PETRICHENKO method.

mSW = plotting point of modern seawater, black filled square; *MOR-I* = predicted seawater chemistry for variations in sea floor spreading rates according to Hardie (1996 and personal communication), unfilled circle marks composition proposed for Badenian seawater; *DOL* = predicted chemistry of seawater affected by the dolomitization of limestones during evaporative concentration. ka= stability field of kainite.

For the Forecarpathian Basin an average value for the Jänecke units of 79.3 ± 2.1 mole percent was determined for Mg, of 7.9 ± 1.3 mole percent for 2K, and of 12.8 ± 1.8 mole percent for SO_4 (table 7). The average values for the East Slovakian Basin with 78.1 ± 1.9 mole percent for Mg, 8.3 ± 1.0 mole percent for 2K, and 13.6 ± 1.5 mole percent for SO_4 are similar, although the two basins are separated by about 200 km. The average m(H_2O)-value of 6080 ± 460 for the 25 Forecarpathian halite samples is clearly higher than the value of 4600 ± 860 for the 18 East Slovakian evaporites, but because the error bars are large, 460 and 860, these differences may not be significant. The m(H_2O)-values indicate that the brines in both basins were saturated with halite but clearly undersaturated with respect to kainite (m(H_2O) ≤1220; Zimmermann, 2000 a); 2 NaCl-values are not available for these samples. If these brines had been evaporated further, kainite would have been precipitated followed by sylvite, kieserite, and carnallite. This is consistent with the mineralogy of the potash beds, which occur locally in the Forecarpathian Basin (Peryt and Kovalevich, 1997).

Upper Miocene (Messinian)

Messinian evaporites are widespread throughout the abyssal plains of the Mediterranean Sea (Hsü, 1973; Nesteroff, 1973) and were drilled at several sites within the Red

TABLE 7

Average seawater compositions in Jänecke units, degrees of evaporation, and DE_{MG}/DE_K-ratios for the Badenian Forecarpathian Basin and East Slovakian Basin

Evaporite basin	DE range	Mg	2K	SO_4	DE_{MG}/DE_K	
East Slovakian Basin	9-17	78.1 ± 1.9	8.3 ± 1.0	13.6 ± 1.5	0.92 ± 0.14	average
		2.4	12.5	10.8	15.0	RSD in %
		18	18	18	18	N
Forecarpathian Basin	12-25	79.3 ± 2.1	7.9 ± 1.3	12.8 ± 1.8	0.99 ± 0.17	average
		2.6	16.4	14.0	17.0	RSD in %
		24	24	24	24	N

DE: Degree of evaporation (based on K)
RSD: relative standard deviation
N: number of samples

Sea (see DSDP, Leg 23). They also crop out in the coastal areas of the Mediterranean (Southern Spain, Sicily, Cyprus, Greece, Israel, Algeria). The thickness of the marine evaporites, which include gypsum, halite and, locally, potash beds, varies between about 200 and 5000 m.

Data sets of primary fluid inclusions in Messinian chevron halite (fig. 4) are available from DSDP sites 225 and 227 in the Red Sea (Kovalevich and others, 1997; Lazar and Holland, 1999), from the Cattolica Basin in Sicily (Ayora, Garçia-Veigas, and Pueyo, 1994b; Garçia-Veigas and others, 1995; Zimmermann, 2000b) and from the Lorca Basin in Spain (Ayora, Garçia-Veigas, and Pueyo, 1994b; Garçia-Veigas and others, 1995; Shepherd and others, 1998).

Red Sea—Kovalevich and others (1997) analyzed primary fluid inclusions in 8 halite samples in relics of chevron and hopper crystals from DSDP sites 225 and 227 close to the axis of the rift east of the Atlantis II Deep using the Petrichenko method

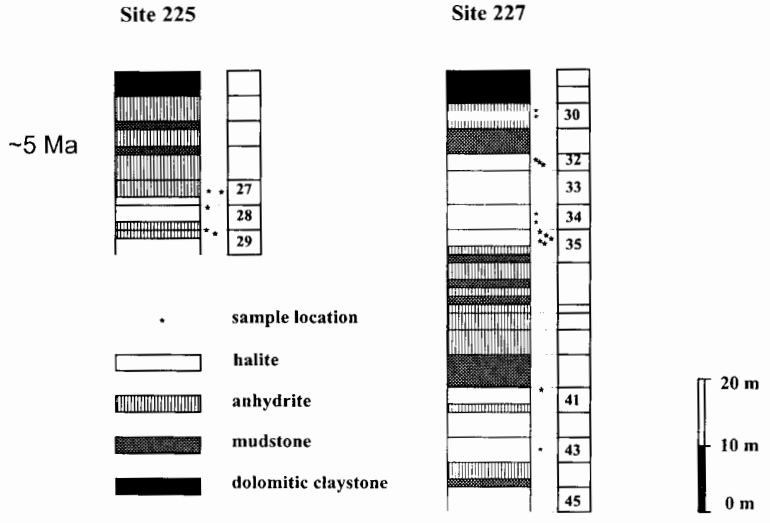

Fig. 12. Sections through the Messinian evaporites of DSDP sites 225 and 227 in the Red Sea indicating the positions of halite sampling. Simplified after Kovalevich, and others (1997).

TABLE 8

Major species concentrations and Jänecke units of fluid inclusions in Messinian marine halite from the Red Sea and the Mediterranean in Sicily and Spain. Data sets from Ayora, Garçia-Veigas, and Pueyo (1994b), Garçia-Veigas and others (1995), Lazar and Holland (1999), Kovalevich and others (1997), and Zimmermann (2000b)

	Basin	site/stratigraphy		sample	method	Na	K	Mg	Ca	Cl	SO_4	CB	Br	Li	B	Rb	Sr	Mg	2K	SO_4	H_2O	2NaCl
						mmol/kg H_2O							mg/kg brine					Jänecke units				
RED SEA I: LAZAR AND HOLLAND (1999)																						
	Red Sea	DSDP-227	ch	30-2/1	Ex-IC	4923	567	493	0	5850	197	3.6	2415					50.6	29.1	20.2	5702	253
sw	Red Sea	DSDP-227	ch	30-2/2	Ex-IC	3520	362	1550	0	6170	479	-2.1	1665					70.1	8.2	21.7	2512	79.6
	Red Sea	DSDP-227	ch	32-1/1	Ex-IC	987	238	3340	0	7510	238	-1.0	3990					90.3	3.2	6.4	1501	13.3
	Red Sea	DSDP-227	ch	32-4/1	Ex-IC	207	93	4639	0	9770	134	-4.7	6370					96.3	1.0	2.8	1152	2.1
sw	Red Sea	DSDP-227	ch	32-4/2	Ex-IC	2910	618	1960	0	6050	598	2.7	2960					68.4	10.8	20.9	1936	50.7
	Red Sea	DSDP-227	ch	34-3/2	Ex-IC	2800	307	1900	0	6320	337	-1.3	2155	25			1270	79.5	6.4	14.1	2322	58.6
	Red Sea	DSDP-227	ch	34-3/3	Ex-IC	2450	306	1990	0	6190	308	-1.0	2510					81.2	6.2	12.6	2265	50.0
	Red Sea	DSDP-227	ch	35-4/1	Ex-IC	5020	325	962	0	6590	349	-0.3	1380					65.3	11.0	23.7	3767	170
sw	Red Sea	DSDP-227	ch	35-5/1	Ex-IC	3500	370	1600	0	6170	490	-1.1	1760					70.3	8.1	21.5	2440	76.9
	Red Sea	DSDP-227	ch	35-5/2	Ex-IC	5000	262	877	0	5980	328	5.6	980					65.6	9.8	24.6	4155	187
sw	Red Sea	DSDP-227	ch	35-5/3	Ex-IC	3630	371	1580	0	6400	536	-4.3	1650					68.7	8.1	23.3	2412	78.9
RED SEA II: KOVALEVICH AND OTHERS (1997)																						
sw	Red Sea	DSDP-227	ch	35-1/110-112	PETRICHENKO			178	1104		299							74.0	6.0	20.0	8281	
	Red Sea	DSDP-227	ch	41-1/125-127	PETRICHENKO			237	945		347							67.0	8.4	24.6	7831	
sw	Red Sea	DSDP-227	ch	43-4/015-017	PETRICHENKO			206	1158		361							71.4	6.4	22.2	9006	
sw	Red Sea	DSDP-225	ch	27-2/110-112	PETRICHENKO			249	1145		231							76.3	8.3	15.4	8327	
sw	Red Sea	DSDP-225	ch	27-2/137-140	PETRICHENKO			217	968		271							71.8	8.1	20.1	7481	
sw	Red Sea	DSDP-225	ch	28-1/062-066	PETRICHENKO			257	1177		274							74.5	8.1	17.3	8763	
	Red Sea	DSDP-225	ch	29-3/069-071	PETRICHENKO			226	1699		362							78.2	5.2	16.7	12068	
	Red Sea	DSDP-225	ch	29-3/101-103	PETRICHENKO			353	1681		391							74.8	7.9	17.4	12480	

SICILY: AYORA AND OTHERS (1994b), GARCIA VEIGAS AND OTHERS (1995), ZIMMERMANN (2000b)																										
sw	Cattolica	Porto-Emp.-38	LU	A	ch	647	EDS-SEM	2470	520	2150		6190	550	0.0							72.6	8.8	18.6	1875	41.7
sw	Cattolica	Siculiana-1	LU	A	ch	745	EDS-SEM	2620	460	2480		6880	580	0.0							75.4	7.0	17.6	1687	39.8
sw	Cattolica	Siculiana-1	LU	A	ch	675	EDS-SEM	2200	470	2500		6490	590	0.0							75.2	7.1	17.7	1669	33.1
sw	Cattolica	Siculiana-1	LU	B	ch	647	EDS-SEM	1360	610	3250		7030	720	0.0							76.0	7.1	16.8	1298	15.9
sw	Cattolica	Realmonte mine	LU	B	ch	3'	EDS-SEM	2430	460	2210		6230	540	0.0							74.2	7.7	18.1	1863	40.8
sw	Cattolica	Porto-Emp.-38	UU	C	ch	340	EDS-SEM	4420	230	800		5790	230	0.0							69.9	10.0	20.1	4848	193
	Cattolica	Realmonte mine	UU	C	ch	11	EDS-SEM	4730	40	440		5370	140	0.0							73.3	3.3	23.3	9251	394
	Cattolica	Realmonte mine	UU	C	ch	11'	EDS-SEM	5100	80	760		6320	190	0.0							76.8	4.0	19.2	5607	258
sw	Cattolica	Realmonte mine	UU	C	ch	13	EDS-SEM	4210	250	1130		6100	310	0.0							72.2	8.0	19.8	3547	135
	Cattolica	Porto-Emp.-38	UU	C	ch	298	EDS-SEM	4600	40	720		6000	40	0.0							92.3	2.6	5.1	7116	295
	Cattolica	Cattolica-5	UU	D	ch	194	EDS-SEM	5430	60	510		6250	130	0.0							76.1	4.5	19.4	8285	405
	Cattolica	Realmonte mine	UU	C	ch	SRe95-08/03	LA-ICPMS, EDS-SEM	5600	100	470		5770	150	9.0	345	2	39	1	32		70.1	7.5	22.4	8285	418
	Cattolica	Realmonte mine	UU	C	ch	SRe95-08/05	LA-ICPMS, EDS-SEM	5660	110	450	10	6090	150	4.6	475	1	21	1	20		69.8	8.5	21.7	8606	439
sw	Cattolica	Realmonte mine	UU	C	ch	SRe95-14/04	LA-ICPMS, EDS-SEM	4770	170	820	10	6050	230	1.4	975	3	41	2	15		72.9	7.6	19.6	4934	212
sw	Cattolica	Realmonte mine	UU	C	ch	SRe95-14/06	LA-ICPMS, EDS-SEM	4690	220	1030	10	5740	310	9.4			49	1	12		71.5	7.6	20.8	3855	163
SPAIN: AYORA AND OTHERS (1994b), GARCIA VEIGAS AND OTHERS (1995), SHEPHERD AND OTHERS (1998)																										
	Lorca	S4	UHU		ch	111	EDS-SEM	3230	200	1120		6390	90	-14.7							85.5	7.6	6.9	4237	123
	Lorca	S4	UHU		ch	112	EDS-SEM	3530	170	1420		6730	130	-6.7							86.9	5.2	8.0	3395	108
	Lorca	S4	UHU		ch	139	EDS-SEM	2130	220	2010		6810	120	-10.1							89.7	4.9	5.4	2478	47.5
	Lorca	S4	LHU		ch	147	EDS-SEM	1210	250	2930		7190	210	-3.9							89.7	3.8	6.4	1700	18.5
	Lorca	S4	LHU		ch	L-147	LA-ICPMS, EDS-SEM	2552	416	3663	17	9626	277	1.4	3340	20	288		17		88.7	5.0	6.3	1344	30.9
	Lorca	S4	LHU		ch	173	EDS-SEM	1420	250	2460		7450	240	-18.5							87.1	4.4	8.5	1965	25.1
	Lorca	S4	LHU		ch	193	EDS-SEM	1600	210	2650		6680	320	-2.9							86.2	3.4	10.4	1805	26.0
	Lorca	S4	LHU		ch	212	EDS-SEM	2130	210	2130		6480	280	-6.5							84.7	4.2	11.1	2207	42.3
	Lorca	S4	LHU		ch	L-212	LA-ICPMS, EDS-SEM	3412	384	3180	13	8536	452	7.5	1927	14	243		9		83.4	5.0	11.5	1457	44.8
	Lorca	S4	LHU		ch	222	EDS-SEM	1950	370	2320		6200	360	0.6							81.0	6.5	12.6	1937	34.0
	Lorca	S4	LHU		ch	226	EDS-SEM	2330	220	2030		6490	350	-8.4							81.5	4.4	14.1	2229	46.8
	Lorca	S4	LHU		ch	228	EDS-SEM	1880	270	2470		6520	350	-1.8							83.6	4.6	11.8	1878	31.8
	Lorca	S4	LHU		ch	229	EDS-SEM	2210	290	2350		6120	380	4.5							81.7	5.0	13.2	1931	38.4
sw	Lorca	S5	LHU	?	ch	127	EDS-SEM	3170	380	1540		5620	490	0.5							69.4	8.6	22.1	2500	71.4
sw	Lorca	S5	LHU	?	ch	134	EDS-SEM	3630	360	1390		5680	440	3.2							69.2	9.0	21.9	2762	90.3
?	Lorca	S5	LHU	?	ch	146	EDS-SEM	4250	310	1010		5670	380	2.3							65.4	10.0	24.6	3593	138

sw: evaporated seawater prior to potash facies (screening based on $DE_{ELEMENT}$ pattern)
ch: hopper crystals or chevrons
CB: charge balance
PETRICHENKO data in g/l. For transformation into mmol/kg H^2O a factor of 1.325 was used.

(Petrichenko, 1973). Lazar and Holland (1999) extracted fluid inclusions (>250 μm) from primary growth bands in 11 halite samples also from DSDP site 227 and analyzed them by ion chromatography (Lazar and Holland, 1988). The two sites are about 10 km apart. At both sites drilling terminated within the Late Miocene evaporite sequence, and cores were taken from the uppermost section of these evaporites. Both sections consist of anhydrite interbedded with halite and some layers of mudstone, but the halite beds do not seem to be correlated (fig. 12). The sequence is topped by a dark gray dolomitic claystone at the boundary of the Early Pliocene. Anhydrite is the dominant mineral at site 225; halite is more abundant at site 227 (fig. 12). At site 225, Kovalevich and others (1997) collected chevron halite from the lower part of the section. Sample 28-1 was collected from a halite bed. The other samples were picked from beds consisting mainly of anhydrite (fig. 12, table 8). At site 227, Kovalevich and others (1997) sampled 2 halite beds from the lower part of the drill core (cores 41 and 43) and 3 samples from the upper halite beds (cores 35 and 33). Lazar and Holland (1999) focused on the top section of the sequence (cores 35, 34, 32, 30; fig. 12).

Some of the fluid inclusion compositions of the Messinian halites from the Red Sea plot in the stability fields of kainite and carnallite, and others close to the projection point of modern seawater (fig. 13). Except for samples 29-3/069-071 and 35-1 with DE_{MG}/DE_K-ratios of 1.4 and 1.2 (table 9), the primary fluid inclusions analyzed by Kovalevich and others (1997) fit the $DE_{ELEMENT}$ pattern for evaporated and Mg-depleted seawater prior to potash facies (Zimmermann, 2000a). Their DE_K ranges from 17 to 33, and DE_{MG}/DE_K-ratios are below 1 (table 10). In the Jänecke diagram at 25°C they are marked as black filled circles and plot close to the path, which represents seawater affected by the dolomitization of limestones (*DOL*, fig. 13).

The average Jänecke units of these inclusions, which contain evaporated seawater prior to potash facies, are 73.8 ± 1.8 mole percent for Mg, 7.2 ± 1.0 mole percent for 2K, and 19.0 ± 2.4 mole percent for SO_4 (table 10). Fluid inclusion compositions of halite from core 29-3 (fig. 12) with high $m(H_2O)$-values above 12000 (table 8; expected value for evaporated and with halite saturated seawater ≤7000-8000) and from sample 41-1, which shows Jänecke units (67.0 mole percent for Mg, 8.4 mole percent for 2K, and 24.6 mole percent for SO_4) significantly different from average are not included in this value.

The situation in the uppermost part of the profile at site 227 investigated by Lazar and Holland (1999) seems to be more complex. Fluid inclusions in halite samples from core 34 (fig. 12) with a DE_K of 29, a DE_{BR} of 43 and 49, with DE_{BR}/DE_K-ratios of 1.5 and 1.7 (table 9) do not show the characteristic $DE_{ELEMENT}$ pattern of evaporated Mg-depleted seawater prior to potash facies (Zimmermann, 2000a). Fluid inclusion compositions of both samples plot within the kainite field (table 8, fig. 13). Their DE_{BR} values below 60 and their $m(H_2O)$-values about 2300 are not consistent with evaporated seawater saturated with kainite ($m(H_2O$ ≤1140; Zimmermann, 2000a). This suggests rather that these inclusion brines have dissolved previously precipitated potash minerals. Anyway, the composition of these primary fluid inclusions cannot be used to constrain the initial composition of seawater in this basin.

The composition of primary fluid inclusions of sample 32-4/2 is particularly interesting. The DE_K of 58 and the DE_{BR} of 60, together with a DE_{MG}/DE_K-ratio below 1 (table 9) indicate that this is evaporated seawater just beginning to precipitate potash minerals. With Jänecke units of 68.4 mole percent for Mg, 10.8 mole percent for 2K, and 20.9 mole percent for SO_4 (table 8), they plot close to modern seawater (Mg=69.0, 2K=6.5, SO_4=24.5) in figure 13. Primary inclusions brines in samples 32-4/1 and 32-1/1 from the same core section (fig. 12) show values for DE_K between 9 and 23; however, their DE_{BR} values vary between 136 and 81 (table 9). This DE is clearly above 60 and suggests the involvement of potash minerals in the origin of these brines. The

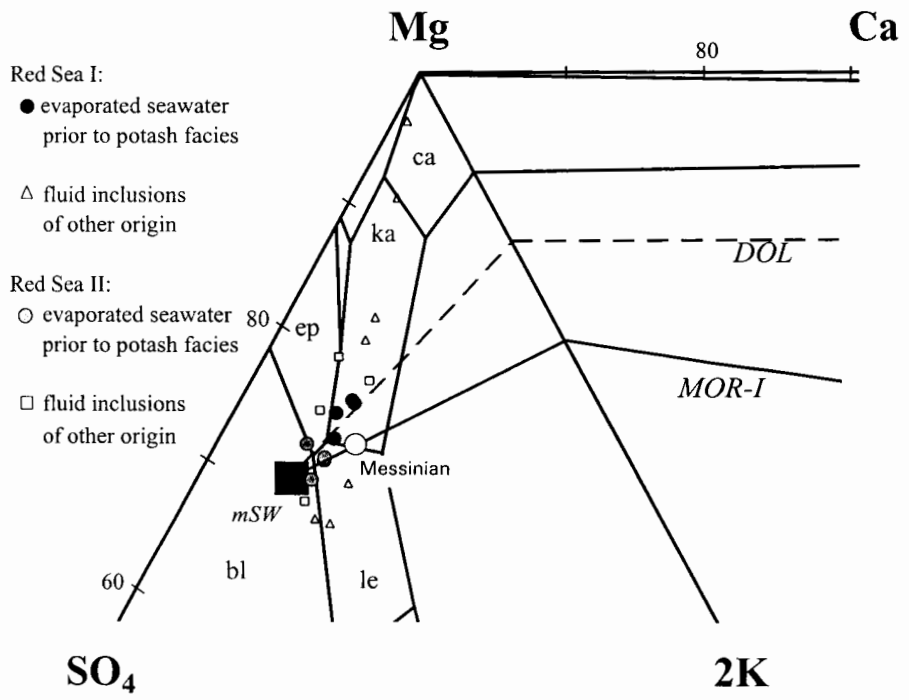

Fig. 13. Compositions of primary fluid inclusions (unfilled triangles and squares) in Messinian marine halites from the Red Sea (Red Sea I: Lazar and Holland, 1999; Red Sea II: Kovalevich, and others, 1997) in the Jänecke plot of the NaCl-KCl-Na_2SO_4-$MgCl_2$-$CaCl_2$-H_2O system at 25°C. Fluid inclusions that fit the $DE_{ELEMENT}$ pattern of evaporated, Mg-depleted seawater prior to potash facies are marked as black or gray filled circles.

mSW = plotting point of modern seawater, black filled square; *MOR-I* = predicted seawater chemistry for variations in sea floor spreading rates according to Hardie (1996 and personal communication), unfilled circle marks composition proposed for Messinian seawater; *DOL* = predicted chemistry of seawater affected by the dolomitization of limestones during evaporative concentration. Stability fields are labeled bl (bloedite), ca (carnallite), ep (epsomite), ka (kainite), le (leonite), sy (sylvite).

compositions of these primary fluid inclusions plot in the stability field of carnallite, and their m(H_2O)-values of 1501 and 1152 and 2NaCl-values of 13 and 2 (table 8) roughly agree with those expected for evaporated seawater precipitating carnallite (m(H_2O) ≤1190, 2NaCl ≤6; Zimmermann, 2000a). It is also striking that the compositions of these fluid inclusions plot exactly on the crystallization path of evaporated seawater (fig. 13). The high bromine concentration of these brines (table 8) also supports that they consist of highly evaporated seawater from which potash minerals. The recycling of evaporites seems to be of minor importance for the evolution of these brines. However, no potash minerals have been reported from the halite beds, in which the analyzed fluid inclusions were trapped. This may suggest that the brines were transported within the primary evaporite basin. Although the analyses of these primary fluid inclusions do not serve to constrain the composition of seawater within the Red Sea Basin during the Messinian, they are fascinating for evaporite petrologists.

The primary fluid inclusions in the remaining samples of cores 35 and 30 fit the $DE_{ELEMENT}$ pattern of evaporated and Mg-depleted seawater prior to potash facies. Their DE_{MG}/DE_K-ratios are below 1, and their values for DE_K range from 20 to 48 (table 9). They are marked as gray filled circles in the Jänecke diagram at 25 ° C and plot slightly shifted from the composition of modern seawater along the path of

TABLE 9

$DE_{ELEMENT}$ patterns of fluid inclusions in Messinian marine halite from the Red Sea and the Mediterranean in Sicily and Spain. Data sets from Ayora, Garçia-Veigas, and Pueyo (1994b), Garçia-Veigas and others (1995), Lazar and Holland (1999), Kovalevich and others (1997), and Zimmermann (2000b)

	Basin	site/stratigraphy		sample	DE_{MG}	DE_{K}	DE_{BR}	DE_{B}	DE_{RB}	DE_{LI}	DE_{MG}/DE_{K}	DE_{BR}/DE_{K}	DE_{B}/DE_{K}	DE_{RB}/DE_{K}	DE_{LI}/DE_{K}
RED SEA I: LAZAR AND HOLLAND (1999)															
	Red Sea	DSDP-227	ch	30-2/1	8.9	53.6	47.8				0.17	0.89			
sw	Red Sea	DSDP-227	ch	30-2/2	28.1	34.2	33.5				0.82	0.98			
	Red Sea	DSDP-227	ch	32-1/1	60.5	22.5	80.6				2.7	3.6			
	Red Sea	DSDP-227	ch	32-4/1	84.1	8.8	135.8				9.6	15.4			
sw	Red Sea	DSDP-227	ch	32-4/2	35.5	58.4	60.2				0.61	1.03			
	Red Sea	DSDP-227	ch	34-3/2	34.4	29.0	42.8			186	1.19	1.47			6.4
	Red Sea	DSDP-227	ch	34-3/3	36.1	28.9	49.4				1.25	1.7			
	Red Sea	DSDP-227	ch	35-4/1	17.4	30.7	28.2				0.57	0.92			
sw	Red Sea	DSDP-227	ch	35-5/1	29.0	35.0	35.4				0.83	1.01			
	Red Sea	DSDP-227	ch	35-5/2	15.9	24.8	19.6				0.64	0.79			
sw	Red Sea	DSDP-227	ch	35-5/3	28.6	35.1	33.6				0.82	0.96			
RED SEA II: KOVALEVICH AND OTHERS (1997)															
sw	Red Sea	DSDP-227	ch	35-1/110-112	20.0	16.8					1.19				
	Red Sea	DSDP-227	ch	41-1/125-127	17.1	22.4					0.76				
sw	Red Sea	DSDP-227	ch	43-4/015-017	21.0	19.5					1.08				
sw	Red Sea	DSDP-225	ch	27-2/110-112	20.8	23.5					0.88				
sw	Red Sea	DSDP-225	ch	27-2/137-140	17.5	20.6					0.85				
sw	Red Sea	DSDP-225	ch	28-1/062-066	21.3	24.3					0.88				
	Red Sea	DSDP-225	ch	29-3/069-071	30.8	21.4					1.44				
	Red Sea	DSDP-225	ch	29-3/101-103	30.5	33.4					0.91				

SICILY: AYORA AND OTHERS (1994b), GARCIA VEIGAS AND OTHERS (1995), ZIMMERMANN (2000b)																
sw	Cattolica (Sicily)	Porto-Emp.-38	A	ch	647	39.0	49.2					0.79				
sw	Cattolica	Siculiana-1	A	ch	745	45.0	43.5					1.03				
sw	Cattolica	Siculiana-1	A	ch	675	45.3	44.4					1.02				
sw	Cattolica	Siculiana-1	B	ch	647	58.9	57.7					1.02				
sw	Cattolica	Realmonte mine	B	ch	3'	40.1	43.5					0.92				
sw	Cattolica	Porto-Emp.-38	C	ch	340	14.5	21.8					0.67				
	Cattolica	Realmonte mine	C	ch	11	8.0	3.8					2.11				
	Cattolica	Realmonte mine	C	ch	11'	13.8	7.6					1.82				
sw	Cattolica	Realmonte mine	C	ch	13	20.5	23.6					0.87				
	Cattolica	Porto-Emp.-38	C	ch	298	13.1	3.8					3.45				
	Cattolica	Cattolica-5	D	ch	194	9.2	5.7					1.63				
	Cattolica	Realmonte mine	C	ch	SRe95-08/03	8.5	9.5	6.8	11.3	15.1	17.6	0.90	0.72	1.19	1.59	1.86
	Cattolica	Realmonte mine	C	ch	SRe95-08/05	8.2	10.4	9.4	6.2	7.9	11.0	0.78	0.90	0.59	0.76	1.05
sw	Cattolica	Realmonte mine	C	ch	SRe95-14/04	14.9	16.1	19.3	11.7	18.2	23.0	0.92	1.20	0.73	1.13	1.43
sw	Cattolica	Realmonte mine	C	ch	SRe95-14/06	18.7	20.8		14.2	14.4		0.90		0.68	0.69	
SPAIN: AYORA AND OTHERS (1994b), GARCIA VEIGAS AND OTHERS (1995), SHEPHERD AND OTHERS (1998)																
	Lorca (Spain)	S4	UHU	ch	111	20.3	18.9					1.07				
	Lorca	S4	UHU	ch	112	25.7	16.1					1.6				
	Lorca	S4	UHU	ch	139	36.4	20.8					1.8				
	Lorca	S4	LHU	ch	147	53.1	23.6					2.2				
	Lorca	S4	LHU	ch	L-147	66.4	39.4	73.7	92.6		164	1.7	1.9	2.4		4.2
	Lorca	S4	LHU	ch	173	44.6	23.6					1.9				
	Lorca	S4	LHU	ch	193	48.0	19.9					2.4				
	Lorca	S4	LHU	ch	212	38.6	19.9					1.9				
	Lorca	S4	LHU	ch	L-212	57.6	36.3	42.1	77.4		114	1.6	1.16	2.1		3.1
	Lorca	S4	LHU	ch	222	42.1	35.0					1.2				
	Lorca	S4	LHU	ch	226	36.8	20.8					1.8				
	Lorca	S4	LHU	ch	228	44.8	25.5					1.8				
	Lorca	S4	LHU	ch	229	42.6	27.4					1.6				
sw	Lorca	S5	LHU ?	ch	127	27.9	35.9					0.78				
sw	Lorca	S5	LHU ?	ch	134	25.2	34.0					0.74				
?	Lorca	S5	LHU ?	ch	146	18.3	29.3					0.62				

sw: evaporated seawater prior to potash facies (screening based on $DE_{ELEMENT}$ pattern)
ch: hopper crystals or chevrons
DE: degree of evaporation
PETRICHENKO data in g/l. For transformation into mmol/kg H^2O a factor of 1.325 was used.

TABLE 10

Average seawater compositions in Jänecke units, degrees of evaporation, and DE_{MG}/DE_K-ratios for the Messinian evaporite basins in the Red Sea, Sicily, and Spain

Evaporite Basin	DE range	Mg	2K	SO_4	DE_{MG}/DE_K	
Red Sea I	34-35	69.3 ± 0.8	8.8 ± 1.2	21.9 ± 0.9	0.90 ± 0.07	average
(Lazar and Holland, 1999)	(60)	1.2	13.6	4.1	7.7	RSD in %
		4	4	4	4	N
Red Sea II	17-24	73.8 ± 1.8	7.2 ± 1.0	19.0 ± 2.4	0.99 ± 0.02	average
(Kovalevich and others, 1997)		2.4	13.9	12.6	2.0	RSD in %
		5	5	5	5	N
Cattolica Basin	44-49	74.7 ± 1.3	7.5 ± 0.7	17.8 ± 0.6	0.94 ± 0.08	average
(Lower Unit)	(58)	1.7	9.3	3.4	8.5	RSD in %
		5	5	5	5	N
Cattolica Basin	16-24	71.6 ± 1.1	8.3 ± 1.0	20.1 ± 0.5	0.81 ± 0.09	average
(Upper Unit)		1.5	12.0	2.5	11.1	RSD in %
		4	4	4	4	N
Lorca Basin	34-36	69.2 ± 0.1	8.8 ± 0.2	22.0 ± 0.1	0.76 ± 0.02	average
		0.1	2.3	0.5	2.6	RSD in %
		2	2	2	2	N
Mediterranean & Red Sea	34-36	72.2 ± 2.2	8.0 ± 0.7	19.8 ± 1.6	0.90 ± 0.08	average
		3	8.8	8.1	8.9	RSD in %
		20	20	20	20	N

DE: Degree of evaporation (based on K and Br when available)
RSD: relative standard deviation
N: number of samples

seawater affected by the dolomitization of limestones (*DOL*, fig. 13). Their average Jänecke units are 69.3 ± 0.8 mole percent for Mg, 8.8 ± 1.2 mole percent for 2K, and 21.9 ± 0.9 mole percent for SO_4 (table 10). Samples 35-3/2, 35-4/1, and 30-2/1 with significantly higher $m(H_2O)$- and 2NaCl values (table 8) are not included in this average, because most likely they have been affected by recycling of halite and brine mixing. The difference in the average of the Jänecke units from the evaporated seawater inclusions studied by Kovalevich and others (1997) and by Lazar and Holland (1999) is not regarded as significant, because these two data sets overlap within the 2σ-range (table 10).

Cattolica Basin (Sicily).—The marine evaporites of the Cattolica Basin in Sicily, which include a potash zone, are the most complete sequence of Messinian evaporites in the Mediterranean. This evaporite sequence is subdivided into the lower Cattolica-Formation and the upper Pasquasia-Formation. The pre-evaporitic unit of the Cattolica Basin consists of diatomitic marls (Tripoli Member; see Garçia-Veigas and others, 1995; Lugli, Schreiber, and Triberti, 1999). These are followed by limestones representing the Calcare di Base and by a thick sequence of cyclic selenitic gypsum. In the central parts of the basin the Cattolica Gypsum is represented by a thin layer of anhydrite overlain by a thick pile of halite beds (~600 m). The chloride facies of the Cattolica-Formation is subdivided into a lower halite unit (unit A), a potash zone including the kainite beds (unit B), and an upper halite unit (units C and D). Lugli, Schreiber, and Triberti (1999) report evidence for a desiccation event between the deposition of units B and C. The kainite beds of unit B have been classically interpreted

as primary. There is evidence that not all of them precipitated directly from evaporated seawater but also formed during the recycling of previously precipitated carnallitic rocks within the sedimentary basin (Zimmermann, 1999). The evaporites of the chloride facies are overlain by a marly sequence (300 m) with up to six cyclic laminated and selenitic gypsum beds (Pasquasia Gypsum Member). Above the Pasquasia Gypsum detrital sediments of brackish or terrestrial origin were deposited, before Pliocene pelagic sediments indicate the inflow of Atlantic seawater (Lugli, Schreiber, and Triberti, 1999).

The evaporites of the lower Cattolica-Formation are of marine origin. There is evidence from $^{87}Sr/^{86}Sr$-ratios in calcium sulfates of the Cattolica-Formation and from the bromine distribution in the halite sequence. $^{87}Sr/^{86}Sr$-ratios of Cattolica-Gypsum (0.70890 ± 0.00003, n=16) and of anhydrite within the halite beds (0.70888 ± 0.00002, n=10) plot on the open-ocean seawater curve for the Messinian (Hodell, Mueller, and Garrido, 1991; Müller and Mueller, 1991). Bromine concentrations of halite range from ~70 μg Br/g halite at the base of unit A to 150 to 200 μg Br/g halite at the bottom of the potash seams in unit B (Decima, 1976). Halite from unit C, which precipitated after the desiccation and the following flooding of the basin, contains 40 to 80 μg Br/g halite (Zimmermann, 2000b). This range agrees well with the Br concentration of the first halite precipitating from evaporated seawater (~10 times concentrated seawater). Only at the very top of the Cattolica-Formation in unit D a progressive influence of continental waters is observed, which is indicated by considerable lower Br concentrations in halite (<<20 μg Br/g halite; Garçia-Veigas and others, 1995).

Primary fluid inclusions in 11 halite samples from units A to D (fig. 14) were analyzed by Ayora, Garçia-Veigas, and Pueyo (1994b) and Garçia-Veigas and others (1995) using cryo-EDS-SEM. They collected 3 samples from Siculiana-I (units A and B), 1 from Cattolica-5 (unit D), 3 from Porto-Empedocle-38 (units A, C, and D), and 4 from the Realmonte mine (units B and C). Cryo-EDS-SEM and laser ablation ICP-MS analyses of primary fluid inclusions are also available from 4 halite samples of unit C in the Realmonte mine (Zimmermann, 2000b). Hopper textures and growth bands of fluid inclusions, indicating primary sedimentation in the evaporite basin, were observed in all the analyzed halite samples. From a stratigraphic point of view the fluid inclusions in the halite samples below the kainite beds (units A and B) and above the desiccation event (unit C) seem to be most promising for tracing the composition of seawater in the Cattolica Basin.

The primary fluid inclusions in halite samples of the lower units A and B (table 9) show the characteristics for evaporated, Mg-depleted seawater prior to potash facies. Their DE_K varies between 44 and 58 (table 9) with DE_{MG}/DE_K-ratios ≤ 1 (table 9). In the Jänecke diagram at 25 °C their compositions are marked as black filled circles. With an average value of 74.7 ± 1.3 mole percent for Mg, 7.5 ± 0.7 mole percent for 2K, and 17.8 ± 0.6 mole percent for SO_4 (table 10), they plot close to the dolomitization path (DOL, fig. 15). They plot in the stability field of kainite distinct from the projection point of modern seawater. Their $m(H_2O)$-values range from 1875 to 1300; 2 NaCl-values from 42 to 16 (table 8), which indicates saturation with halite but not with kainite ($m(H_2O) \leq 1140$; $2NaCl \leq 13$). However, inclusion brines in sample 3' are close to the saturation with kainite. If further evaporated, kainite followed by carnallite and kieserite would precipitate from these brines.

The compositions of primary fluid inclusions in halite samples from upper units C and D show significantly lower values of DE_K between 4 and 24 (table 9), which might suggest precipitation from only mildly concentrated seawater. But the DE_{MG}/DE_K-ratios between 1.6 and 3.5 of the fluids in samples 11 and 11' from the Realmonte mine, in sample 194 from Cattolica-5, and in 298 from Porto-Empedocle-38 (table 9),

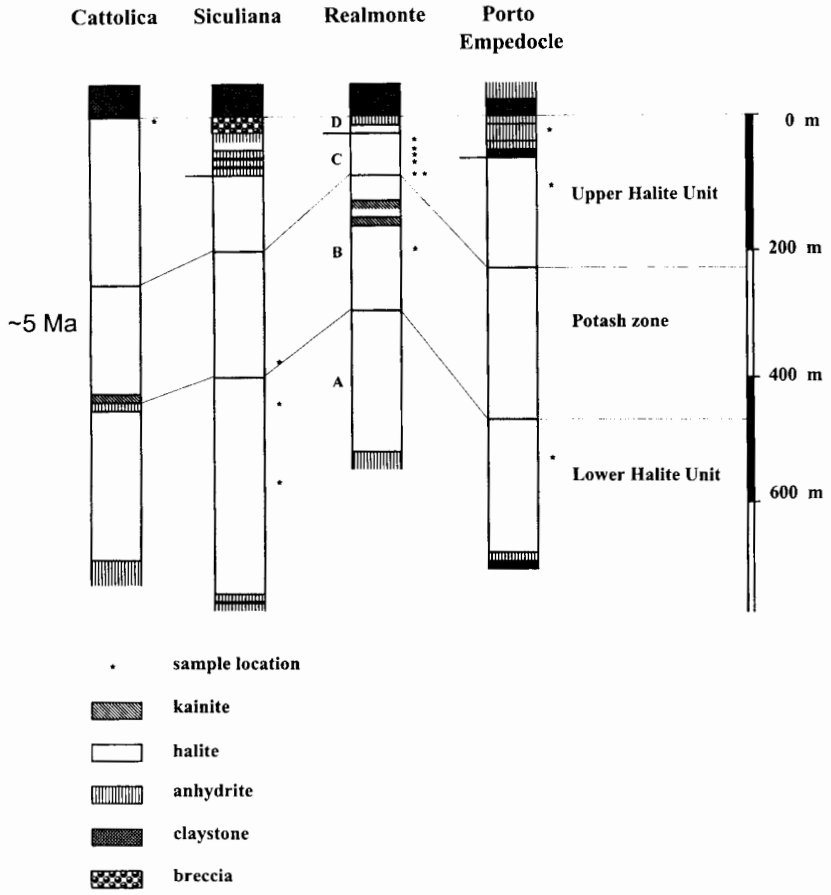

Fig. 14. Sections through the Messinian evaporites of the Cattolica Basin in Sicily indicating the positions of halite sampling. Simplified after Garçia-Veigas, and others (1995).

indicate that these brines are not simply evaporated seawater prior to potash mineral precipitation (Zimmermann, 2000a). The fluid inclusions plot in the stability fields of carnallite and epsomite (fig. 14). They are most likely reaction fluids from the dissolution of carnallite or kainite mixed with more dilute, NaCl-saturated waters.

In unit C, above the desiccation event, only 5 samples (13, 08/03, 08/05, 14/04, 14/06) from Realmonte mine and 1 sample of Porto-Empedocle-38 (340) remain as candidates for evaporated, in magnesium depleted seawater prior to potash facies (DE_K=10-24, DE_{MG}/DE_K<1; see table 9). m(H_2O)-values above 8000, and relatively high 2 NaCl-values above 400 for primary fluid inclusions in samples 08/03 and 08/05 may indicate the recycling of halite. Therefore, they were not added to the set of primary fluid inclusions, which is used for the reconstruction of the chemistry of Messinian seawater in the Cattolica Basin. The remaining primary fluid inclusions of chevron halite in unit C are marked as gray filled circles in the Jänecke diagram at 25°C. They plot distinct from the composition of modern seawater along the trend predicted for seawater, which is affected by the dolomitization of limestones (*DOL*, fig. 15). m(H_2O)-values of inclusion brines between 3547 and and 2NaCl-values between 135 and 212 indicate their saturation with respect to halite. But they inclusion fluids

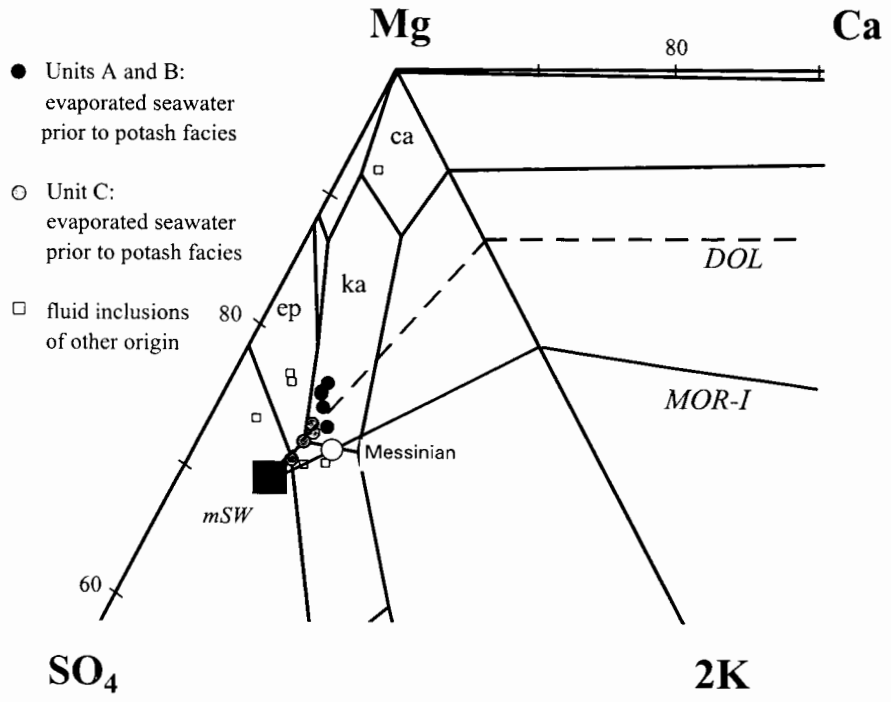

Fig. 15. Compositions of primary fluid inclusions (unfilled squares) in Messinian marine halites from the Cattolica Basin (Sicily; units A and B below potash beds, unit C upper halite above desiccation features) in the Jänecke plot of the NaCl-KCl-Na_2SO_4-$MgCl_2$-$CaCl_2$-H_2O system at 25°C. Fluid inclusions that fit the $DE_{ELEMENT}$ pattern of evaporated, Mg-depleted seawater prior to potash facies are marked as black or gray filled circles.

mSW = plotting point of modern seawater, black filled square; *MOR-I* = predicted seawater chemistry for variations in sea floor spreading rates according to Hardie (1996 and personal communication), unfilled circle marks composition proposed for Messinian seawater; *DOL* = predicted chemistry of seawater affected by the dolomitization of limestones during evaporative concentration. Stability fields are labeled ca (carnallite), ep (epsomite), ka (kainite).

are far from saturation with respect to potassic salts. Their average Jänecke units are 71.6 ± 1.1 mole percent for Mg, 8.3 ± 1.0 mole percent for 2K, and 20.1 ± 0.5 mole percent for SO_4 (table 10). The Jänecke units of inclusions of evaporated seawater in halite from above the kainite beds (unit C) differ slightly from the ones in halite from below the potash seams (units A, B), but there is an overlap within the 2σ-range (table 10).

Lorca Basin (Spain).—The Lorca Basin (fig. 4), one of the intermontane basins of the Eastern Bethic Chain, contains a sequence of Messinian sediments, which consists of basal diatomitic marls (100 m), marine halite (<235 m), and an upper unit of laminated gypsum (60 m; see Garçia-Veigas and others, 1995). Whereas borehole S4, located in the central part of the basin, cut a 235m-thick sequence of evaporites, borehole S5, only some 2 km away, penetrated only 49 m of the evaporite sequence in a more marginal position in the basin. The evaporite deposit in borehole S4 can be divided into a lower halite unit and an upper unit similar to the Cattolica evaporites in Sicily. However, kainite beds do not seem to occur in the Lorca Basin (Garçia-Veigas and others, 1995). The bromine content of the halite in the upper unit is below 20 μg Br/g halite and is comparable to the bromine concentrations in halite of unit D in the Cattolica Basin. The bromine concentrations in the lower halite unit range from 40 to

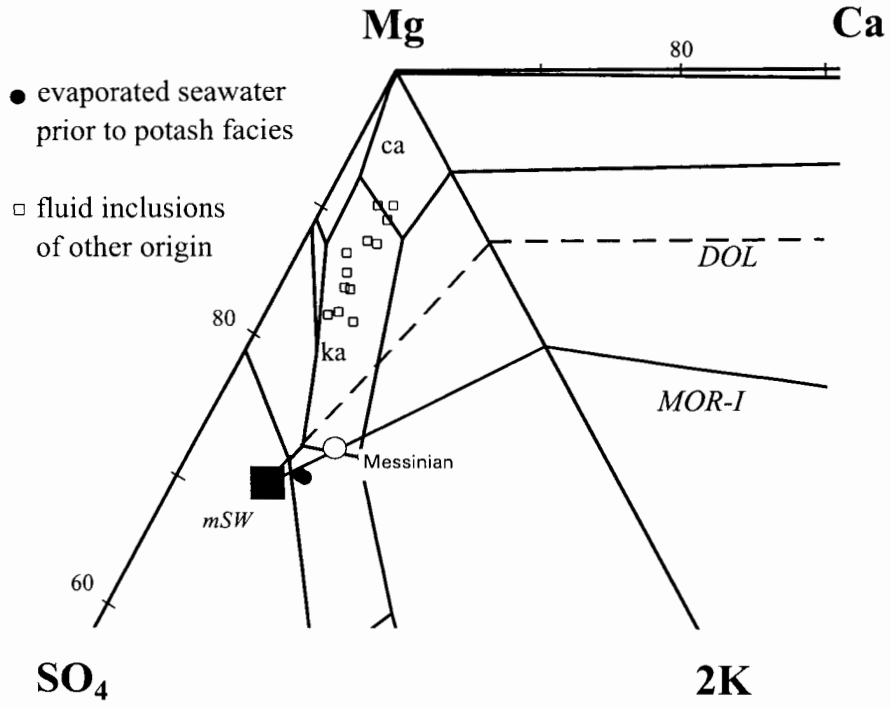

Fig. 16. Compositions of primary fluid inclusions (unfilled squares) in Messinian marine halites from the Lorca Basin (Spain) in the Jänecke plot of the NaCl-KCl-Na_2SO_4-$MgCl_2$-$CaCl_2$-H_2O system at 25°C. Fluid inclusions that fit the $DE_{ELEMENT}$ pattern of evaporated, Mg-depleted seawater prior to potash facies are marked as black filled circles.

mSW = plotting point of modern seawater, black filled square; *MOR-I* = predicted seawater chemistry for variations in sea floor spreading rates according to Hardie (1996 and personal communication), unfilled circle marks composition proposed for Messinian seawater; *DOL* = predicted chemistry of seawater affected by the dolomitization of limestones during evaporative concentration. Stability fields are labeled ca (carnallite) and ka (kainite).

70 μg Br/g halite and are similar to the concentrations in halite in unit C above the kainite beds. Bromine concentrations of 150 to 200 μg Br/g halite as in halite from Sicily below the kainite beds have not been reported from the Lorca Basin. Although the correlation of the two evaporite sequences over a distance of hundreds of kilometers is uncertain, the processes that led to the deposition of the evaporites in the Lorca Basin (LHU and UHU) and to the sedimentation of the upper unit in the Cattolica Basin (UU, units C and D) were similar.

Garçia-Veigas others (1995) analyzed primary fluid inclusions from chevrons and hopper crystals in 14 halite samples from the Lorca Basin using cryo-EDS-SEM. They collected 8 halite samples from the LHU in borehole S4, 3 samples from the UHU in borehole S4, and 3 halite samples from borehole S5 (possibly LHU). Samples 212 and 147 in S4 were also analyzed by LA-ICP-MS (L147, L212; Shepherd and others, 1998).

With the exception of the fluids in halite samples from S5, the compositions of primary fluid inclusions in Lorca halite plot in the kainite field or close to its border with the sylvite and carnallite fields of the Jänecke diagram at 25 °C (fig. 16). The DE_K of all primary fluid inclusions in S4 halite are below 60 (DE_K =16-39; table 9), whereas the few existing data for Br, B, and Li indicate DE 's above 60. The DE_{MG}/DE_K-ratios of these inclusion brines vary between 1.1 and 2.2 (table 9). These $DE_{ELEMENT}$ patterns do not fit for evaporated, in magnesium depleted seawater prior to potash facies.

$m(H_2O)$-values vary between 1340 and 4240, 2NaCl-values between 19 and 123 (table 8). This indicates saturation with halite but not with kainite. Therefore it seems likely that these fluid inclusions represent brines that have dissolved carnallite or kainite, similar to the brines in core 34 at DSDP site 227 in the Red Sea. The fluid inclusion compositions of the UHU ($m(H_2O)$=2478-4237, 2NaCl=48-123) are slightly more dilute than the brine inclusions from the LHU in S4 ($m(H_2O)$=1344-2229, 2NaCl=19-46; table 8). This trend accounts for an increasing influence of dissolution of evaporites by halite saturated brines toward the end of evaporitic period in this basin.

According to Garçia-Veigas and others (1995) the halite samples of the more marginal borehole S5 can be correlated with the base of the halite sequence in drillhole S4. However, their primary fluid inclusions are very different in composition. Although their DE_K between 29 and 36 (table 9) are similar to the values in primary fluid inclusions from S4, their DE_{MG}/DE_K-ratios are significantly below 1. They fit the $DE_{ELEMENT}$ pattern for evaporated, in magnesium depleted seawater prior to potash facies. These fluid inclusion compositions are marked as black filled circles in the Jänecke diagram at 25 °C (fig. 16). With 69.2 ± 0.1 mole percent for Mg, 8.8 ± 0.2 mole percent for 2K, and 22.0 ± 0.1 mole percent for SO_4 (table 10) they plot close to present-day seawater and slightly below the path of seawater affected by the dolomitization of limestones (*DOL*, fig. 16).

Figure 17 shows the average composition of evaporated seawater prior to potash mineral precipitation in the Red Sea, in the Cattolica Basin (Sicily), and in the Lorca Basin (Spain). Their Jänecke units cover a range between 69.3 and 74.7 mole percent for Mg, between 7.2 and 8.8 mole percent for 2K, and between 17.8 and 22.0 mole percent for SO_4. The difference in seawater composition between the 3 basins does not seem to be significant. The composition of average seawater in Messinian evaporite basins, with Jänecke units of 72.2 mole percent for Mg, 8.0 mole percent for 2K, and 19.8 mole percent for SO_4 (table 10), plots on the dolomitization path just within the kainite field (DOL, fig. 17). This is consistent with the mineralogy of the kainite beds in Sicily.

DISCUSSION AND CONCLUSIONS

In all the studies reported here special care was taken to use only primary fluid inclusions from marine halite that contains chevron structures. Nevertheless, a great variety in fluid inclusion compositions was observed. This is partly due to syndepositional mineral reactions in the primary evaporite basin. A considerable fraction of the halite precipitated from brines that had dissolved earlier potash beds. This process is not only seen in halite beds related to potash zones (for example the upper halite unit of the Navarra Basin) but also in evaporite sequences that do not seem to contain potash beds (for example, the Lorca Basin and the Red Sea). Either, potash minerals were precipitated in these basins and were then completely redissolved, or they are still present, but undiscovered. The latter possibility implies brine transportation within these basins. Although fluid inclusions that have been affected by the dissolution of potash minerals do not help to constrain the composition of unevaporated seawater within evaporite basins, they yield extremely valuable information regarding the salt forming processes in such basins.

It was shown that the composition of primary fluid inclusions in Tertiary marine halites cannot be explained simply in terms of the evaporative concentration of modern seawater or of seawater with higher Mg/Ca-ratios up to 10 (fig. 5). They are also not consistent with Hardie's (1996 and personal communication, see fig. 18) proposed significant changes in global seawater composition during the Tertiary. In order to test the dolomitzation model for Phanerozoic seawater, which suggests that the composition of seawater can be explained in terms of variations in the degree of dolomitization of limestone during the evaporative concentration of seawater, primary

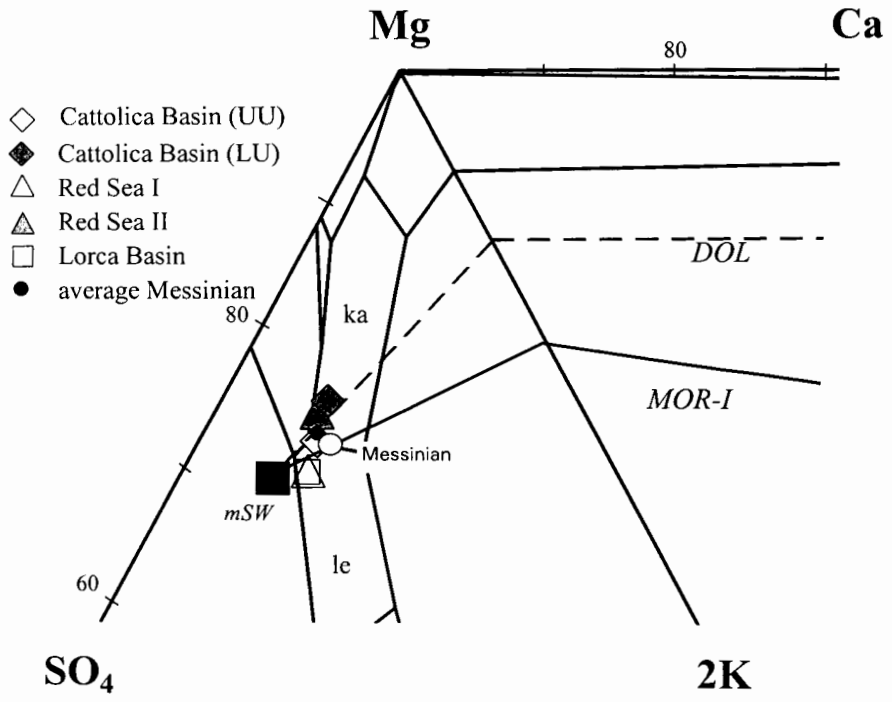

Fig. 17. Average seawater compositions in different Messinian evaporite basins in the Jänecke plot of the system NaCl-KCl-Na_2SO_4-$MgCl_2$-$CaCl_2$-H_2O at 25°C. Red Sea I: Lazar and Holland, 1999; Red Sea II: Kovalevich, and others, 1997; UU: upper unit above desiccation features; LU: Lower unit below potash beds. Black filled circle marks average seawater composition of all the Messinian evaporite basins studied.

mSW = plotting point of modern seawater, black filled square; *MOR-I* = predicted seawater chemistry for variations in sea floor spreading rates according to Hardie (1996 and personal communication), unfilled circle marks composition proposed for Messinian seawater; *DOL* = predicted chemistry of seawater affected by the dolomitization of limestones during evaporative concentration. Stability fields are labeled ka (kainite) and le (leonite).

fluid inclusions were screened (based on DE_K, DE_{BR}, DE_{MG}/DE_K) for evaporated and Mg-depleted seawater prior to potash facies. Primary fluid inclusions in 69 of 130 halite samples fit these geochemical criteria. In the Jänecke diagram (based on Mg, 2K, SO_4, $m(H_2O)$, 2NaCl) at 25°C, all plot along the path predicted for Phanerozoic seawater affected by dolomitization during evaporative concentration (*DOL*, see fig. 18). The primary fluid inclusions in these 69 samples of marine halite are used to constrain the composition of unevaporated seawater in several Tertiary evaporite basins.

As estimated from the Jänecke diagram, Eocene seawater in the Navarra Basin was depleted in magnesium by 27 to 33 percent compared to modern seawater. The degree of Mg-depletion, calculated from the ratio of DE_{MG} to DE_K (Zimmermann, 2000a), ranges from 19 to 39 percent (table 11). According to Zimmermann (2000a), the mineralogy of $MgSO_4$-free sylvite beds followed by carnallite beds is consistent with unevaporated Eocene seawater, which compared to modern seawater is depeleted in magnesium of by 33 to 35 percent. This means an average Mg-depletion of 31 percent relative to modern seawater for Eocene seawater in the Navarra Basin (table 11).

Compared to modern seawater the Oligocene seawater in the Mulhouse Basin was depleted in magnesium by 36 to 38 percent estimated on the basis of DE_{MG}/DE_K-ratios of basal fluid inclusions (table 11). The mineralogy of the sylvite beds followed by magnesium-sulfate-free carnallite beds indicates a Mg-depletion of at least 33 percent.

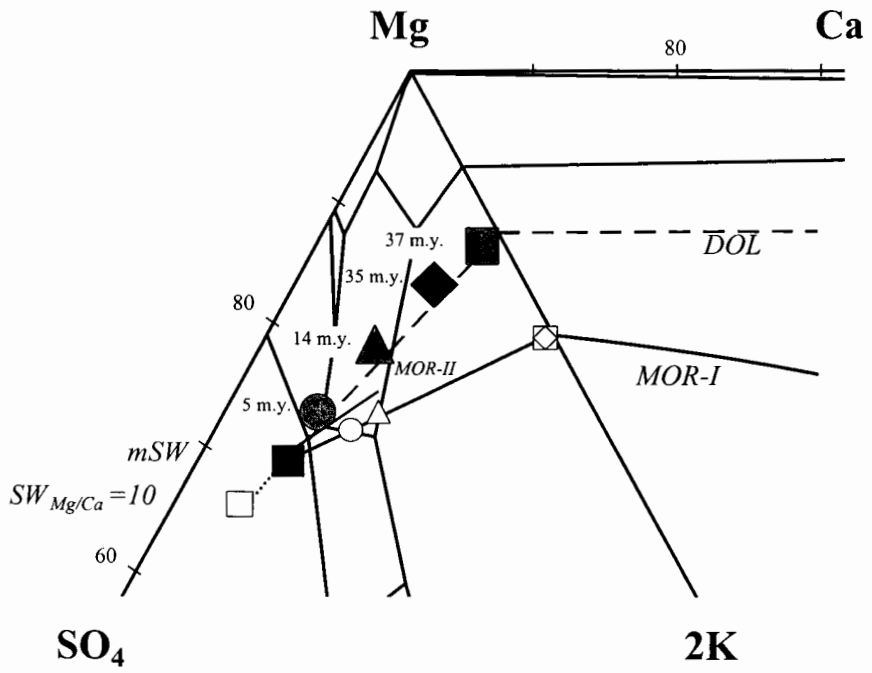

Fig. 18. Evolution of seawater chemistry during the past 40 Ma (gray filled symbols) based on analyses of primary fluid inclusions in marine halite of several Tertiary (Upper Eocene to Upper Miocene) evaporite basins in the Jänecke plot of the system NaCl-KCl-Na_2SO_4-$MgCl_2$-$CaCl_2$-H_2O at 25°C.

mSW = plotting point of modern seawater, black filled square; $SW_{Mg/Ca=10}$ = plotting point of seawater with an initial Mg/Ca-ratio of 10; *MOR-I* = predicted seawater chemistry for variations in sea floor spreading rates according to Hardie (1996 and personal communication), unfilled symbols marks composition proposed for Eo-/Oligocene, Badenian and Messinian seawater; *MOR-II* = predicted seawater chemistry, if affected by variations in sea floor spreading rates, according to Holland, Horita, and Seyfried (1996); *DOL* = predicted chemistry of seawater affected by the dolomitization of limestones during evaporative concentration.

Because some of the fluid inclusions contain a small amount of $CaCl_2$, the upper estimate for Mg-depletion of these brines is slightly in excess of 35 percent. This implies the precipitation of tachhydrite after further evaporation. This mineral has not been reported from the Mulhouse Basin potash beds. It may, however, have been present in the sequence and later dissolved. The Jänecke diagram indicates between 34 and 40 percent depletion in magnesium. The average estimate for the depletion in Mg in Oligocene seawater of the Mulhouse Basin is 36 percent relative to modern seawater.

According to the Jänecke plot Badenian seawater from the Carpathian region was depleted in magnesium by 20 percent compared to modern seawater (table 11). The mineralogy of the potash zone suggests depletion in magnesium between 15 and 22 percent. The large analytical error of the Petrichenko method makes it difficult to obtain a precise value for the Mg-depletion based on DE_{MG}/DE_K-ratios. Analyses based on this technique suggest a magnesium depletion of 8 ± 14 percent in Badenian seawater from the East Slovakian Basin. Altogether it seems reasonable that the magnesium deficit in Badenian seawater was about 20 percent (table 11).

The mineralogy of the potash zone in the Cattolica Basin evaporites suggests depletion in magnesium of 11 to 15 percent of Red Sea and Mediterranean seawater compared to modern seawater (table 11). The estimate of Mg-depletion from $DE_{MG}/$

TABLE 11

Magnesium depletion of seawater compared to modern seawater in evaporite basins through the Tertiary (37-5 Ma) estimated from the DE_{MG}/DE_K-ratios and Jänecke units of fluid inclusions in halite and from the mineralogy of the potash zone

Sample/stratigraphy		DE	Mg-depletion in mol%				Time	Basin
			DE_{MG}/DE_K	Jänecke	potash	average	ma	
BI-425	LHU	53	36	30	33-35			
BI-430	LHU	49	39	27	33-35			
BI-436	LHU	38	19	30	33-35			
BI-437	LHU	34	28	33	33-35			
			31 ± 9	30 ± 2	34	32 ± 2	37	Navarra Basin
19.79		46	36	34	33-37			
20.50		35	38	40	33-37			
			37 ± 1	37 ± 3	35	36 ± 1	35	Mulhouse Basin
ESB/FCB		9-25	8/1 ?	20	15-22			
				20	19	20 ± 1	14	Carpathian Basins
Red Sea I		34-35	10	5	11-15			
Red Sea II		17-24	1	15	11-15			
Sicily	LU	44-49	6	15	11-15			
Sicily	UU	16-24	19	11	11-15			
Lorca		34-36	24	5	11-15			
			12 ± 9	10 ± 5	13	12 ± 2	5	Mediterranean & Red Sea

DE: Degree of evaporation (based on K and Br when available)
LU: Lower Unit
UU: Upper Unit
LHU: Lower Halite Unit
FCB: Forecarpathian Basin
ESB: East Slovakian Basin
Red Sea I: Lazar and Holland (1999)
Red Sea II: Kovalevich and others (1997)

DE_K-ratios scatters between 1 and 24 percent with an average value of 12 ± 9, whereas the Jänecke units give values between 5 and 15 percent with an average of 10 ± 5 (table 11). If the dolomitization of limestones was an important process in this basin, the average estimate for magnesium depletion compared to modern seawater is 12 percent (table 11).

Altogether the composition of evaporated seawater in Tertiary marine halite plots along a path indicating depletion in Mg and SO_4 in a 1:1 molar ratio (*DOL*, fig. 18). The depletion in magnesium relative to modern seawater varies from 31 to 36 percent in the Lower Oligocene and Upper Eocene, to 20 percent in the Badenian, and 12 percent in the Messinian throughout the Mediterranean and Red Sea. This trend suggests increasing Mg-depletion of seawater with increasing age during the Tertiary (fig. 19). If the increase in the Mg content of seawater since the Eocene represents a global trend based on a Mg concentration of 55 mmole/kg H_2O in modern seawater, this translates into Mg concentrations of 38 ± 2 mmole/kg H_2O for Upper Eocene seawater, of 35 ± 2 mmole/kg H_2O for Lower Oligocene seawater, of 44 ± 2 mmole/kg H_2O for Lower-Middle Miocene seawater, and of 49 ± 4 mmole/kg H_2O for Upper Miocene seawater (fig. 19).

If we assume (in lack of a more acceptable assumption) no variation for the past 40 Ma in the accumulation of carbonate and calcium-sulfate during the evaporative concentration of seawater (that is, constant $\{m_{Ca}+2 - \frac{1}{2} m_{HCO_3}\}$ in initial seawater), this would imply SO_4 concentrations of 10 ± 1 mmole/kg H_2O and 11 ± 1 mmole/kg

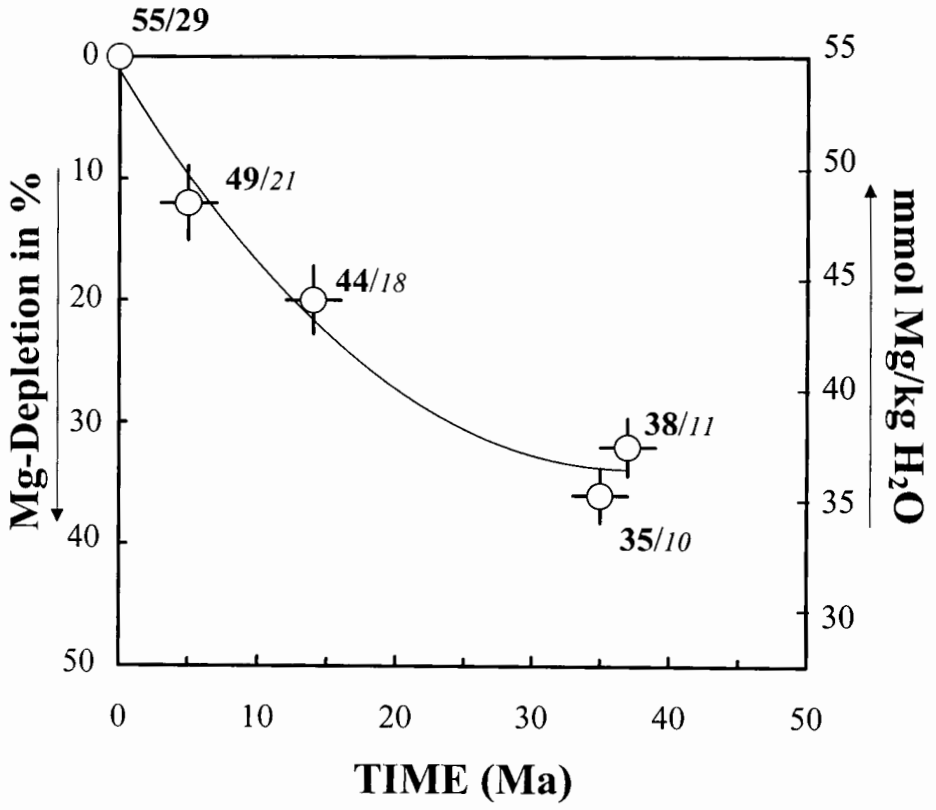

Fig. 19. Magnesium depletion of seawater (mole percent) relative to modern seawater and Mg concentration in unevaporated seawater in Tertiary sedimentary basins against time in million years (Ma).

Values next to data points represent Mg and SO_4-concentrations of unevaporated seawater in mmole/kg H_2O. These estimates are based on concentrations of 55 mmole Mg/H_2O und 29 mmole SO_4/kg H_2O in modern seawater. Sulfate concentrations in unevaporated seawater printed in italic are estimated (in lack of a more acceptable *assumption*) on the basis of the amount of carbonate and calcium-sulfate accumulating during the evaporative concentration of present-day seawater.

H_2O for Upper Eocene and Lower Oligocene seawater, of 18 ± 1 mmole/kg H_2O for Lower-Middle Miocene seawater, and of 21 ± 1 for Upper Miocene seawater (fig. 19, values in italics).

Without data sets from evaporite basins of the same age from different parts of the globe it is difficult to say unequivocally whether the observed changes in magnesium depletion in the basins investigated to date are global or regional. The different degrees of $MgSO_4$-depletion of the inclusion fluids could be due either to differences in the amount of dolomitization of limestone during the evaporative concentration of modern seawater in the several evaporite basins or due to changes in the composition of seawater as a whole, or due to a combination of these effects. Analyses of fluid inclusions containing unevaporated seawater are needed to determine the cause of the observed $MgSO_4$-depletion; fluid inclusions in marine calcite cements may help to resolve the issue.

If the observed variations in Tertiary seawater composition are global, the changes raise the question as to what processes have driven them and why the increase in magnesium in seawater during the past 40 Ma has been coupled with an equimolar increase in the sulfate concentration. If the differences are due to regional processes

within evaporite basins prior to halite precipitation, a shift has occurred in this set of basins from highly dolomitizing environments during the Upper Eocene and Lower Oligocene to low or minor dolomitization environments during the Badenian and Messinian.

The simplest way to account for the observed differences in magnesium and sulfate depletion between the several Tertiary basins is in terms of differences in the exposure of the brines to calcite and/or aragonite along their evaporation path. Dolomitization is apt to be extensive when seawater passes across large carbonate platforms on its way to basins where halite and potash minerals are deposited. Dolomitization is apt to be minor when seawater has little contact with $CaCO_3$ sediments prior to evaporation to the halite facies and beyond. There is, however, little evidence that such geographical differences are responsible for the observed changes in the composition of the brines in the Tertiary basins described in this study. In any case, it would be most fortuitous if the necessary differences in geography were sufficiently regular to yield the observed gradual progressive change in the Mg and SO_4 content of the brines during the past 40 Ma.

It is therefore more likely that all or a large part of the observed difference in the composition of the brines during the past 40 Ma is due to changes in the composition of seawater as a whole. Changes in the operation of two mechanisms for the removal of magnesium and sulfate from seawater may have been responsible for the proposed alterations: the cycling of seawater through seafloor basalt and the formation of dolomite in shallow water carbonates.

Hardie (1996 and personal communication) has proposed that even small changes in the rate of seawater cycling through midocean ridges can produce large changes in the composition of the global oceans. Holland, Horita, and Seyfried (1996) have calculated that the effects are much smaller. If their estimate is correct, the global variation in seawater composition due to changes in seawater cycling through mid-ocean ridges alone is not sufficient to explain the observed changes particularly in the Upper Eocene and Lower Oligocene. During the past 40 Ma there is little evidence for large changes in the rate of seafloor spreading (Lithgow-Bertelloni and others, 1993; Heller, Anderson, and Angevine, 1996). Therefore it is more likely that the changes in seawater composition are related to the progressive increase in $CaCO_3$ deposition in the deep sea, where dolomitization is minor, coupled with a progressive decrease in the rate of shallow water $CaCO_3$ deposition, where dolomitization is common. This hypothesis is discussed at length in a forthcoming paper (Holland and Zimmermann, 2000).

ACKNOWLEDGMENTS

I am particularly grateful to Professor H. D. Holland for his support and his critical comments, which very much helped to improve this manuscript. The author gratefully acknowledges K. C. Benison and an anonymous reviewer for their constructive comments and J. Pasteris for her careful editorial handling of the manuscript. Funding for this project was provided by NASA (NAG5-4174) and by the Deutsche Forschungsgemeinschaft (Zi 418/1).

REFERENCES

Althammer W., 1924, Die graphische und rechnerische Behandlung von Salzlösungen: Kali-Forschungs-Anstalt Staβfurt-Leopoldshall, 57 p.

D'Ans J., 1933, Die Lösungsgleichgewichte des Systems der Salze ozeanischer Salzablagerungen: Kali-Forschungs-Anstalt Berlin, Verlagsges. fuer Ackerbau mbH, 254 p.

Ayora, C., and Fontarnau, R., 1990, X-ray microanalysis of frozen fluid inclusions at -140 °C: Chemical Geology, v. 89, p. 135-148.

Ayora, C., Garçia-Veigas, J., and Pueyo, J.-J., 1994a, The Chemical and hydrological evolution of an ancient potash-forming evaporite basin as constrained by mineral sequence, fluid inclusion composition, and numerical simulation: Geochimica et Cosmochimica Acta, v. 58, p. 3379-3394.

—— 1994b, X-ray microanalysis of fluid inclusions and its application to the geochemical modelling of evaporite basins: Geochimica et Cosmochimica Acta, v. 58, p. 43-55.

Baar, A., and Kühn, R., 1962, Der Werdegang der Kalisalzlagerstätten am Oberrhein: Neues Jahrbuch Mineralogie, Abhandlungen, v. 97, p. 289-336.

Benison, K. C., and Goldstein, R. H., 1999, Permian paleoclimate data from fluid inclusions in halite: Chemical Geology, v.154, p. 113-132.

Blanc-Valleron, M.-M., ms, 1991, Les formations paléogènes évaporitiques du bassin de Mulhouse et des bassins plus septentrionaux d'Alsace: Thèse Doct Etat, Strasbourg et document BRGM, Orléans, 204 p.

Blanc-Valleron, M.-M. and Schuler, M., 1997, The Salt Basins of Alsace, *in* Busson, G. and Schreiber, B., editors, Sedimentary Deposition in Rift and Foreland Basins in France and Spain: New York, Columbia University Press, p. 95-135.

von Borstel, L. E., Zimmermann, H., and Ruppert, H., 2000, Fluid inclusion studies in modern halite from the Inagua salt work: Netherlands, Den Hague, Conference Volume, SALT 2000- 8th World Symposium on Salt, May 7-11, 2000, v. 2, p. 673-678.

Braitsch O., 1962, Entstehung und Stoffbestand der Salzlagerstätten: Berlin-Göttingen-Heidelberg, Springer, 232p.

Braitsch, O., and Herrmann, A. G., 1964, Zur Geochemie des Broms in salinaren Sedimenten. Teil II: Die Bildungstemperaturen primärer Sylvin- und Carnallitgesteine: Geochimica et Cosmochimica Acta, v. 28, p. 1081-1109.

Brantley, S. L., Crerar, D. A., Møller, N., and Weare, J. H., 1984, Geochemistry of a modern marine evaporite: Bocana de Virrilá, Peru: Journal of Sedimentary Petrology, v. 54, p. 447-462.

Bruland, K. W., 1983, Trace elements in seawater: Chemical Oceanography, v. 8, p. 157-220.

Busson, G., Cornée, A., Dulau, N., Fontes, J. Ch., Geisler, D., Gouleau, D., Jaccard, J., Landry, J. C., Noël, D., Perthuisot, J. P., Pierre, C., Poumot, C., Tetard, J., Thomas, J. C. Thomas, M., Trauth, N., and Zaninetti, L.,1982, Données hydrochimiques, biologiques, isotopiques, sédimentologiques et diagénétiques sur les marais salants de Salin-de-Giraud (Sud de la France): Geologie mediterranéenne, IX, v. 4, p. 303-391.

Canals, A., Carpentier, B., Huc, A. Y., Guilhaumou, N., and Ramsey, M. H., 1993, Microanalysis of primary fluid inclusions in halite; constraints for an evaporitic sedimentation modeling; application to the Mulhouse Basin (France) : Organic Geochemistry, v. 20, 8, p. 1139-1151.

Cendón, D. I., Ayora, C. I., and Pueyo, J.-J., 1998, The origin of barren bodies in the Subiza potash deposit, Navarra, Spain: Implications for sylvite formation: Journal of Sedimentary Research, v. 68, p. 43-52.

Claypool, G. E., Holser, W. T., Kaplan, I. R., Sakai, H., and Zak, I., 1980, The age curves of sulfur and oxygen isotopes in marine sulfate and their mutual interpretation: Chemical Geology, v. 79, p. 199-260.

Das N., Horita J., and Holland H. D., 1990, Fluid inclusions in halite from the Salina Group of the Michigan Basin: implications for Late Silurian seawater and the origin of sedimentary brines: Geochimica et Cosmochimica Acta, v. 54, p. 319-327.

Decima, A., 1976, Initial data on bromine distribution in the Miocene salt formation of southern Sicily: Società Geologica Italiana Memoric, v. 16, p. 39-43.

Fontes, J. C., Filly, A., Gaudant, J., and Duringer, P., 1991, Origine continentale des évaporites paléogènes de haute Alsace: arguments paléoécologiques, sédimentologiques et isotopiques: Bulletin de la Société Géologique de France, v. 162, p. 725-737.

Galamay, A. R., and Karoli, S., 1997, Geochemistry of the Badenian salts from the East Slovakian Basin, Slovakia: Slovak Geological Magazine, v. 3, 3, p. 187-192.

Galamay, A.R., Bukowski, K., and Przybyło, J., 1997, Chemical composition and origin of brines in the Badenian evaporite basin of the Carpathian Foredeep: fluid inclusion data from Wieliczka (Poland): Slovak Geological Magazine, v. 3, 2, p. 165-171.

Garçia-Veigas, J., Orti, F., Rossel, L., Ayora, C., Rouchy, J.-M., and Lugli, S., 1995, The Messinian salt of the Mediterranean: geochemical study of the salt from the Central Sicily Basin and comparison with the Lorca Basin (Spain): Bulletin de la Société Géologique de France, v. 166, p. 699-710.

Garçia Veigas, J., Rossel, L., and Garlicki, A., 1997, Petrology and geochemistry (fluid inclusions) of Miocene halite rock salts (Badenian, Poland): Slovak Geological Magazine, v. 3, 3, p. 181-186.

Garlicki, A., and Wiewiórka, J., 1981, The distribution of bromine in some halite rocks of the Wieliczka salt deposit (Poland): Annales de la Société Géologique de Pologne, v. 51, p. 353-359.

Goldstein, R. H., and Reynolds, T. J., 1994, Systematics of Fluid Inclusions in Diagenetic Minerals: Tulsa, Oklahoma, Society for Sedimentary Geology, Short Course 31, 199 p.

Harvie C. E., Møller N. E., and Weare J. H., 1984, The prediction of mineral solubilities in natural waters: the Na-K-Mg-Ca-H-Cl-SO_4-OH-HCO_3-CO_3-CO_2-H_2O system to high ionic strengths at 25 °C: Geochimica et Cosmochimica Acta, v. 48, p. 723-751.

Hardie, L. A., 1996, Secular variation in seawater chemistry: An explanation for the coupled variation in the mineralogies of marine limestones and potash evaporites over the past 600 m.y: Geology, v. 24, p. 279-283.

Heller, P.L., Anderson, D.L., and Angevine, C.L., 1996, Is the middle Cretaceous pulse of rapid sea-floor spreading real or necessary?: Geology, v. 24, p. 491-494.

Herrmann, A. G., Knake, D., Schneider, J., and Peters, H., 1973, Geochemistry of modern seawater and brines from saltpans: Main components and bromine distribution: Contributions to Mineralogy and Petrology, v. 40, p. 1-24.

Hodell, D. A., Mueller, P. A., and Garrido, J. R., 1991, Variation in the strontium isotopic composition of seawater during the Neogene: Geology, v. 19, p. 24-27.

Hofmann, P., Huc, A. Y., Carpentier, B., Schaeffer, P., Albrecht, P., Keely, B., Maxwell, J. R., Sinninghe Damsté, J.S., de Leeuw, J. W., and Leythaeuser, D., 1993, Organic matter of the Mulhouse Basin, France: a synthesis: Organic Geochemistry, v. 20, p. 1105-1123.

Holland, H. D., 1978, The chemistry of the atmosphere and the oceans: New York, John Wiley and Sons, 351 p.

Holland, H. D., Horita, J., and Seyfried, W. E., 1996, On the secular variations in the composition of Phanerozoic marine potash evaporites: Geology, v. 24, p. 993-996.

Holland, H. D., and Zimmermann, H., 1998, On the secular variations in the composition of Phanerozoic marine potash evaporites: comment and reply: Geology, v. 26, p. 91-92.

—— 2000, The dolomite problem revisited: International Geology Review, v. 42, p. 481-490.

Hsü, K. J., 1973, The desiccated deep-basin model for the Messinian events: *in* Drooger C. W. (ed.) Messinian Events in the Mediterranean: Amsterdam, Koninklijke Nederlandse Akademie Van Wetenschappen, p. 60-67.

Isele C., ms, 1998, Element- und Isotopenfraktionierung bei der Evaporitbildung in der Meerwassersaline von Ibiza (Balearen, Spanien): Diplomarbeit, unveröffentlicht, Institut für Geologie und Dynamik der Lithosphäre, Universität Göttingen, 66 p.

Johnson, W. J., and Goldstein, R. H., 1993, Cambrian sea water preserved as fluid inclusions in marine low-magnesium calcite cement: Nature, v. 362, p. 335-337.

Kühn, R., and Roth, H., 1979, Beiträge zur Kenntnis der Salzlagerstätte am Oberrhein: Zeitschrift für Geologische Wissenschaften, v. 7, p. 953-966.

Kovalevich, V. M., Jarmolowicz-Szulc, K., Peryt, T. M., and Poberegski, A.V., 1997, Messinian chevron halite from the Red Sea (DSDP sites 225 and 227): fluid inclusion study: Neues Jahrbuch Mineralogie, Monatshefte, v. 10, p. 433-450.

Kovalevich, V. M., and Petrichenko, O. I., 1997, Chemical composition of brines in Miocene evaporite basins of the Carpathian region: Slovak Geological Magazine, v. 3, 3, p. 173-180.

Lazar, B., and Holland, H. D., 1988, The analysis of fluid inclusions in halite: Geochimica et Cosmochimica Acta, v. 52, p. 485-490.

Lazar, B. and Holland, H. D., ms, 1999, Fluid inclusion analyses of Messinian chevron halite in the Red Sea (DSDP site 227).

Lithgow-Bertelloni, C., Richards, M.A., Ricard, Y., O'Connell, R.J., and Engebretson, D.C., 1993, Toroidal-poloidal partitioning of plate motions since 120 MA: Geophysical Research Letters, v. 20, p. 375-378.

Lowenstein, T. K., and Spencer, R. J., 1990, Syndepositional Origin of Potash Evaporites: Petrographic and Fluid Inclusion Evidence: American Journal of Science, v. 290, p. 1-42.

Lugli, S., Schreiber, B. C., and Triberti, B., 1999, Giant Polygons in the Realmonte Mine (Agrigento, Sicily): Evidence for the Desiccation of a Messinian Halite Basin: Journal of Sedimentary Research, v. 69, 3, p. 764-771.

McCaffrey, M. A., Lazar, B., and Holland, H. D., 1987, The Evaporation Path of Seawater and the Coprecipitation of Br^- and K^+ with Halite: Journal of Sedimentary Petrology, v. 57, p. 928-937.

Müller, D. W., and Mueller, P. A., 1991, Origin and age of the Mediterranean evaporites: implications from Sr isotopes: Earth and Planetary Science Letters, v.107, p. 1-12.

Nesteroff, W. D., 1973, Un modèle pour les évaporites messinienes en Méditerranée: des bassin peu profonds avec dépôts d'évaporites lagunaires, *in* Drooger C. W., editor, Messinian Events in the Mediterranean: Amsterdam, Koninklijke Nederlandse Akademie Van Wetenschappen, p. 68-81.

Ortí, F., 1997, Evaporitic Sedimentation in the South Pyrenean Foredeeps and the Ebro Basin During the Tertiary: A General View, *in* Busson, G. and Schreiber, B., editors, Sedimentary Deposition in Rift and Foreland Basins in France and Spain: New York, Columbia University Press, p. 319-334.

Peryt, T. M., Karoli, S., Peryt, D., Petrichenko, O. I., Przemyslaw, G., Narkewicz, W., Durkovicova, J., and Dobieszynska, Z., 1997, Westernmost occurrence of the Middle Miocene Badenian gypsum in central Paratethys (Koberice, Moravia, Czech Republic): Slovak Geological Magazine, v. 3 (2), p. 105-120.

Peryt, T. M., and Kovalevich, V. M., 1997, Association of redeposited salt breccias and potash evaporites in the Lower Miocene of Stebnyk (Carpathian Foredeep, West Ukraine): Journal of Sedimentary Research, v. 67, p. 916-925.

Peters H., ms, 1988, Stoffbestand und Genese des Kaliflözes Riedel (K3Ri) im Salzstock Wathlingen-Hänigsen, Werk Niedersachsen-Riedel: Dissertation, Universität Göttingen, 231 p.

Petrichenko, O. I., 1973, Methods of Study of inclusions in minerals of saline deposits: Naukova dumka, Kiev, 90 p. (in Ukrainian, translated *in* Fluid Inclusions Research, Proceedings of Current Research on Fluid Inclusions, v. 12, p. 214-274, 1979).

Petrychenko, O. I., Peryt, T. M., and Roulston, B., ms, 2000, Seawater composition during deposition of Viséan evaporites in the Moncton Subbasin of New Brunswick as inferred from the fluid inclusion study of halite, submitted to Canadian Journal of Earth Sciences.

Poutoukis, D., ms, 1991, Hydrochimie, teneurs isotopiques et origine des saumures associées aux gisements de Potasse d'Alsace: Thèse, Université Paris-Sud, 140 p.

Rosell, L. and Pueyo, J.-J., 1997, Second Marine Evaporitic Phase in the South Pyrenean Foredeep: The Priabonian Potash Basin (Late Eocene: Autochthonous-Allochthonous Zone), *in* Busson, G. and Schreiber, B., editors, Sedimentary Deposition in Rift and Foreland Basins in France and Spain: New York, Columbia University Press, p. 358-387.

Schuler, M., ms, 1988/90, Environnements et paléoclimats paléogènes. Palynologie et biostratigraphie de l'Eocène et de l'Oligocène inférieur dans les fossés rhénan, rhodanien et de Hesse : Thèse Doctorale Etat, Université Strasbourg, 339 p.

Shaidetska, V. S., 1997, Geochemistry of Neogene evaporites of the Transcarpathian Trough in Ukraine: Slovak Geological Magazine, v. 3, 3, p. 193-200.

Shepherd, T. J., Ayora, C., Cendón, D. I., Chenery, S. R., and Moissette, A., 1998, Quantitative solute analysis of single fluid inclusions in halite by LA-ICP-MS and cryo-SEM-EDS: complementary microbeam techniques: Journal of European Mineralogy, v. 10, p. 1097-1108.

Shepherd, T. J., and Chenery, S. R., 1995, Laser ablation ICP-MS elemental analysis of individual fluid inclusions: An evaluation study: Geochimica et Cosmochimica Acta, v. 59, p. 3997-4007.

Sissingh, W., 1998, Comparative Tertiary Stratigraphy of the Rhine Graben, Bresse Graben and Molasse Basin: Correlation of Alpine foreland events: Tectonophysics, v. 300, p. 249-284.

Usdowski, E., and Dietzel, M., 1998, Atlas and Data of Solid-Solution Equilibria of Marine Evaporites: Springer-Verlag, 316 p.

Williams-Stroud, S. C., 1994, Solution to the Paradox? Results of Some Chemical Equilibrium and Mass Balance Calculations Applied to the Paradox Basin Evaporite Deposit: American Journal of Science, v. 294, p. 1189-1228.

Zimmermann, H., 1999, The Miocene Kainite Beds of Sicily - Their Origin and Constraints on Seawater Composition in the Evaporative Basin: EOS, Transactions, American Geophysical Union, 1999 Fall Meeting, v. 80., no. 46, November 16, 1999/Supplement, p. F515.

—— 2000a, On the origin of fluid inclusions in Phanerozoic halite - basic interpretation strategies: Geochimica et Cosmochimica Acta, in press.

—— ms, 2000b, The evolution of seawater during the past 40 Ma – evidence from the mineralogy of marine evaporites and fluid inclusions in marine halite: Habilitationsschrift, Universität Göttingen, 206 p.